

## CHAPTER II

### COEXISTENCE OF TWO NEMATIC PHASES IN MIXTURES OF ROD-LIKE AND DISC-LIKE COMPOUNDS

#### 2.1 INTRODUCTION

When two nematogens, one with rod-like and the other with plate-like molecules are mixed together, purely for geometrical reasons, the plate-like molecules can be expected to align with their short axes perpendicular to the long axes of the rod-like molecules. This can result in a biaxial phase if both the rod-like and plate-like molecules are themselves orientationally ordered in mutually orthogonal directions. There have been many theoretical studies on the thermodynamics of mixtures of rod-like and plate-like molecules. Most of these theories confirm the occurrence of a biaxial phase, even though the pure components composing the mixture themselves exhibit only uniaxial phases. Alben (1973) and Caflisch et al. (1984) have made calculations based on a lattice model and obtained phase diagrams exhibiting a biaxially ordered phase (see for e.g., Fig. 2.1). Chen and Deutch (1984) developed a special lattice model considering both short-range repulsions and long-range Van der Waals like attractions and again obtained phase diagrams similar to that shown in Fig. 2.1. Rabin et al. (1982) have also presented a theory of liquid crystal mixtures made up of rod-like and plate-like molecules. They consider continuous orientations unlike the lattice models which consider discrete orientations. The phase diagrams obtained by them

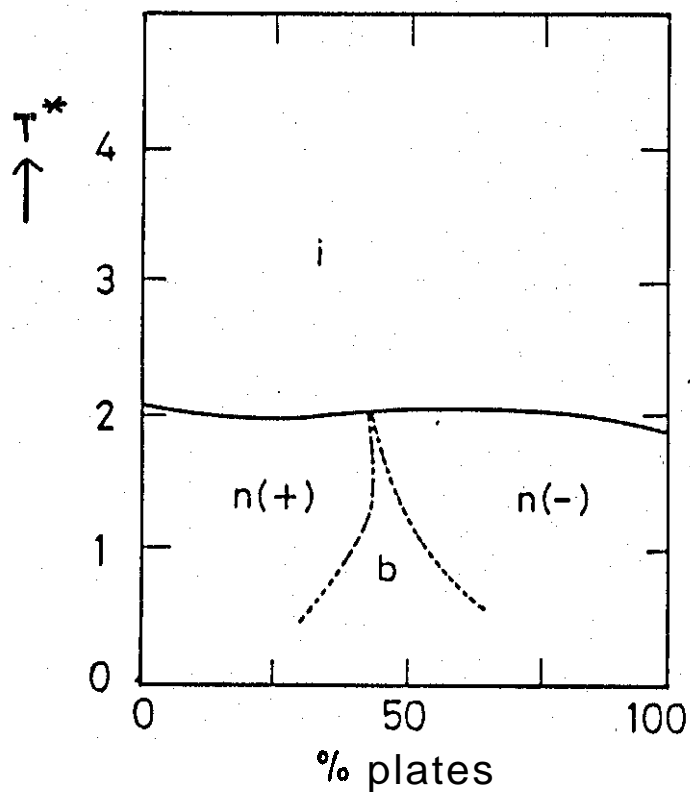


Figure 21

Theoretically predicted phase diagram of mixtures of rods (with  $l = 5$ ) and plates (with  $W = 3$ ).  $i$ : isotropic,  $n(+)$ : positive uniaxial phase,  $n(-)$ : negative uniaxial phase,  $b$ : biaxial phase,  $T^*$ : effective temperature. (From Alben 1973).

are once again similar to Fig. 2.1.

Yu and Saupe (1980) have indeed observed a biaxial phase in an amphiphilic system composed of potassium laurate, decanol and water in a concentration and temperature range separating two uniaxial phases, one composed of disc-shaped micelles and the other of rod-shaped micelles (Fig. . However, in this case the shape of the micelle itself changes with temperature and can presumably take that of a biaxial ellipsoid in the range of existence of the biaxial nematic phase.

In any case the micelles are not rigid structures with identical shapes and volumes. However all the theoretical models mentioned earlier are applicable to rigid molecules. We therefore wanted to investigate the possibility of occurrence of a biaxial phase in a thermotropic mixture of rod-like and disc-like liquid crystalline compounds. Nematogens made up of rod-like molecules have been known for a long time but compounds with disc-like molecules which exhibit the nematic phase were synthesized only recently (Tinh et al. 1979).

Earlier observations had indicated that the discotic nematic ( $N_D$ ) is not miscible with the classical nematic ( $N_R$ ) made up of rod-like molecules (Tinh et al. 1979, 1981). Tinh et al. (1981) studied some mixtures of the discotic nematogen hexaheptyloxybenzoate of triphenylene ( $C_7$ OHBT) with the rod-like nematogen bis-heptyloxybenzoate (BHB) and found that a 75:25 mixture by weight of  $C_7$ OHBT and BHB directly goes over to the isotropic phase from the crystalline

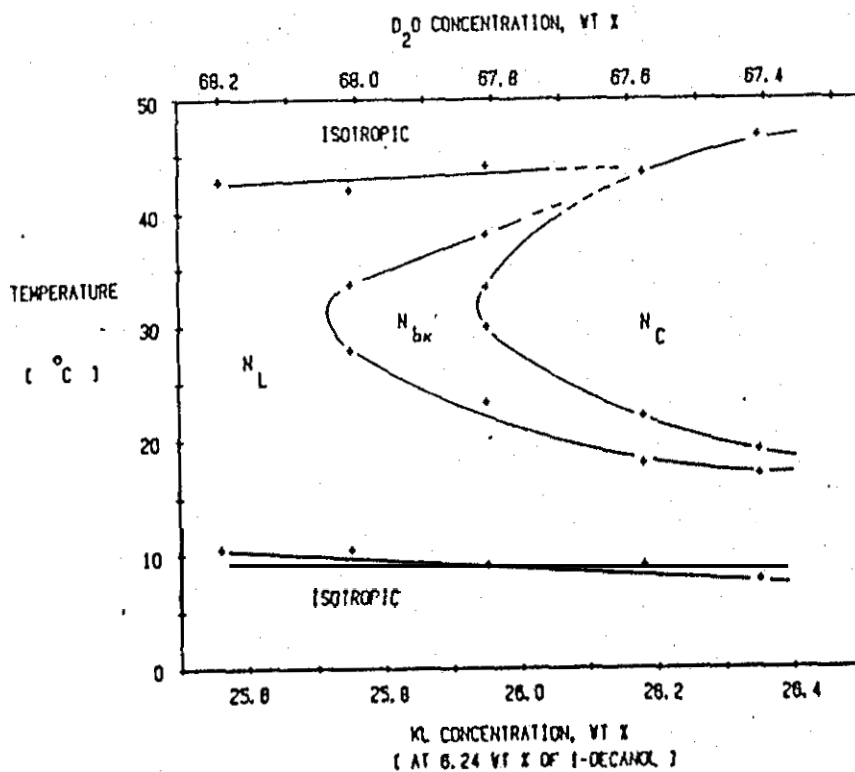


Figure 2.2

Phase diagram of potassium laurate and 1-decanol - D<sub>2</sub>O system. N<sub>L</sub> : positive uniaxial, N<sub>c</sub> : negative uniaxial, N<sub>bx</sub> : biaxial phase (From Yu and Saupe 1980).

state without going through any mesophase. Apart from these results there have been no detailed studies on phase diagrams of mixtures composed of compounds with rod-like and disc-like molecules.

We have for the first time studied experimentally the phase diagrams of two such systems. Instead of the biaxial phase predicted by the theories mentioned above, we found the coexistence of the two nematic phases, i.e.,  $N_R$  which is rich in the rod-like compound and  $N_D$  which is rich in the disc-like compound.

Soon after our observation of the coexistence of the two uniaxial phases, we were gratified to come across the work of Palffy-Muhoray et al. (1984, 1985a, 1985b) which theoretically predicts such a coexistence. In the following section we therefore give an outline of their theory.

In this theory, the Maier-Saupe pseudo potential expressed in a rotationally invariant form has been generalised to binary mixtures. The component order parameters, phase diagrams and coexistence curves have been determined. This theory also leads to induced biaxiality but this coincides with the spinodal region and is found to be unstable in comparison with uniaxial phase separation. The two coexisting phases are found to be lower in free energy than the biaxial one.

Let us consider a binary mixture containing  $N_1$  molecules of species 1 and  $N_2$  molecules of species 2 confined in a volume  $V$ . The

single particle pseudo potential generalised to a two component mixture is

$$\begin{aligned} \epsilon(\hat{n}_1) = & -\frac{1}{2} \gamma_{11} \rho_1 - \frac{1}{2} \gamma_{12} \rho_2 - \left[ \frac{2}{3} u_{11} \rho_1 S_{\alpha\beta}^{(1)} \right. \\ & \left. + \frac{2}{3} u_{12} \rho_2 S_{\alpha\beta}^{(2)} \right] \times \left[ \sigma_{\alpha\beta}^{(1)} - \frac{1}{2} S_{\alpha\beta}^{(1)} \right] \end{aligned} \quad (2.1)$$

Here  $\hat{n}_1$  is the unit vector with components  $n_\alpha^{(1)}$  specifying the orientation of a molecule of species 1,  $\rho_1$  and  $\rho_2$  are the number densities of the two species,  $\gamma_{ij}$  and  $u_{ij}$  are isotropic and anisotropic interaction strengths between molecules of species  $i$  and  $j$ .  $\sigma_{\alpha\beta}^{(i)} = \frac{1}{2} [3n_\alpha^{(i)} n_\beta^{(i)} - 1]$  and  $S_{\alpha\beta}^{(i)} = \langle \sigma_{\alpha\beta}^{(i)} \rangle$  is the order parameter of species  $i$  where  $\langle \rangle$  denotes the ensemble average. The single particle pseudo potential for molecules of species 2 is obtained by interchanging the indices in eqn. (2.1). The Helmholtz free energy density of the system is given by

$$\begin{aligned} F = & -kT \left[ \rho_1 \ln \left\{ \frac{1}{\rho_1} \int \exp[-\epsilon(\hat{n}_1)/kT] d\Omega \right\} \right. \\ & \left. + \rho_2 \ln \left\{ \frac{1}{\rho_2} \int \exp[-\epsilon(\hat{n}_2)/kT] d\Omega \right\} \right] \end{aligned} \quad (2.2)$$

where  $d\Omega$  is an element of solid angle. The equilibrium order parameter  $S_{\alpha\beta}^{(i)}$  ( $i = 1, 2$ ) is obtained by minimising the free energy. Such a minimisation leads to the self-consistent eqn.

$$S_{\alpha\beta}^{(i)} = \frac{\int \sigma_{\alpha\beta}^{(i)} \exp[-\epsilon(\hat{n}_i)/kT] d\Omega}{\int \exp[-\epsilon(\hat{n}_i)/kT] d\Omega} \quad (2.3)$$

A proper theory of mixtures requires evaluation of the chemical potentials. Palfy-Muhoray et al. have calculated the chemical potentials of the constituent species and examined the possibility of coexistence. The chemical potentials are obtained by differentiation of the free energy with respect to the particle number. If the volume of the system is  $V = V_1 N_1 + V_2 N_2$ , where  $V_i$  and  $N_i$  are the molecular volume and the number of molecules of species  $i$ , the chemical potential of species 1 is obtained as

$$\begin{aligned}
 \mu_1 = & -kT \ln \left[ \frac{1}{\rho_1} \int \exp[-\epsilon(\hat{n}_1)/kT] d\Omega \right] + kT \rho_2 (V_2 - V_1) \\
 & - \frac{1}{2} \rho_2 [\gamma_{11} \rho_1 V_2 - \gamma_{12} (\rho_1 V_1 - \rho_2 V_2) - \gamma_{22} \rho_2 V_1] \\
 & - \frac{1}{3} \rho_2 [u_{11} \rho_1 V_2 s_{\alpha\beta}^{(1)} s_{\beta\alpha}^{(1)} - u_{12} (\rho_1 V_1 - \rho_2 V_2) s_{\alpha\beta}^{(1)} s_{\beta\alpha}^{(2)} \\
 & - u_{22} \rho_2 V_1 s_{\alpha\beta}^{(2)} s_{\beta\alpha}^{(2)}] \quad (2.4)
 \end{aligned}$$

The chemical potential for species (2) is obtained by interchanging the indices 1 and 2.

Two coexisting phases with different compositions occur when the chemical potential of each species is the same in both the phases, at the same temperature.

The equilibrium state for the binary mixture at a given temperature and composition is either a single phase or two coexisting phases, depending on the global minimum of the free energy.

To locate the points of coexistence the absolute activity

$\lambda_1 = \exp(\mu_1/kT)$  of species 1 is plotted versus the absolute activity  $\lambda_2 = \exp(\mu_2/kT)$  of species 2, the composition being a parameter along the curve. These curves may intersect with each other or with themselves and the points of intersection indicate the points of possible coexistence: at such a point two phases A and B with compositions  $Y_{1A}$  and  $Y_{1B}$  have the same activity and chemical potential for each component. The straight lines, which are tangent to the free energy density versus composition curves, and pass through two distinct points identify the compositions where two phase coexistence is possible. However this coexistence is **realised** only if this construction represents the lowest possible free energy of the system (Fig. 2.3).

Palfy-Muhoray et al. found that in a binary mixture of rods and plates the free energy density of the system in the two coexisting uniaxial phases is lower than that of the biaxial phase. Their temperature composition phase diagram for a binary nematic mixture is shown in Fig. 2.4. We see that unlike in the previous theoretical models which predict biaxiality, this theory leads to the coexistence of two uniaxial nematic phases.

Hashim et al. (1984) have carried out Monte Carlo computer simulation studies on such mixtures. In their model the particles are confined to the sites of a simple cubic lattice and for an equimolar mixture, each rod-like particle has six plates as nearest neighbours and vice versa. They have arrived at the result that the equimolar mixture of rods and plates separates into two uniaxial nematic

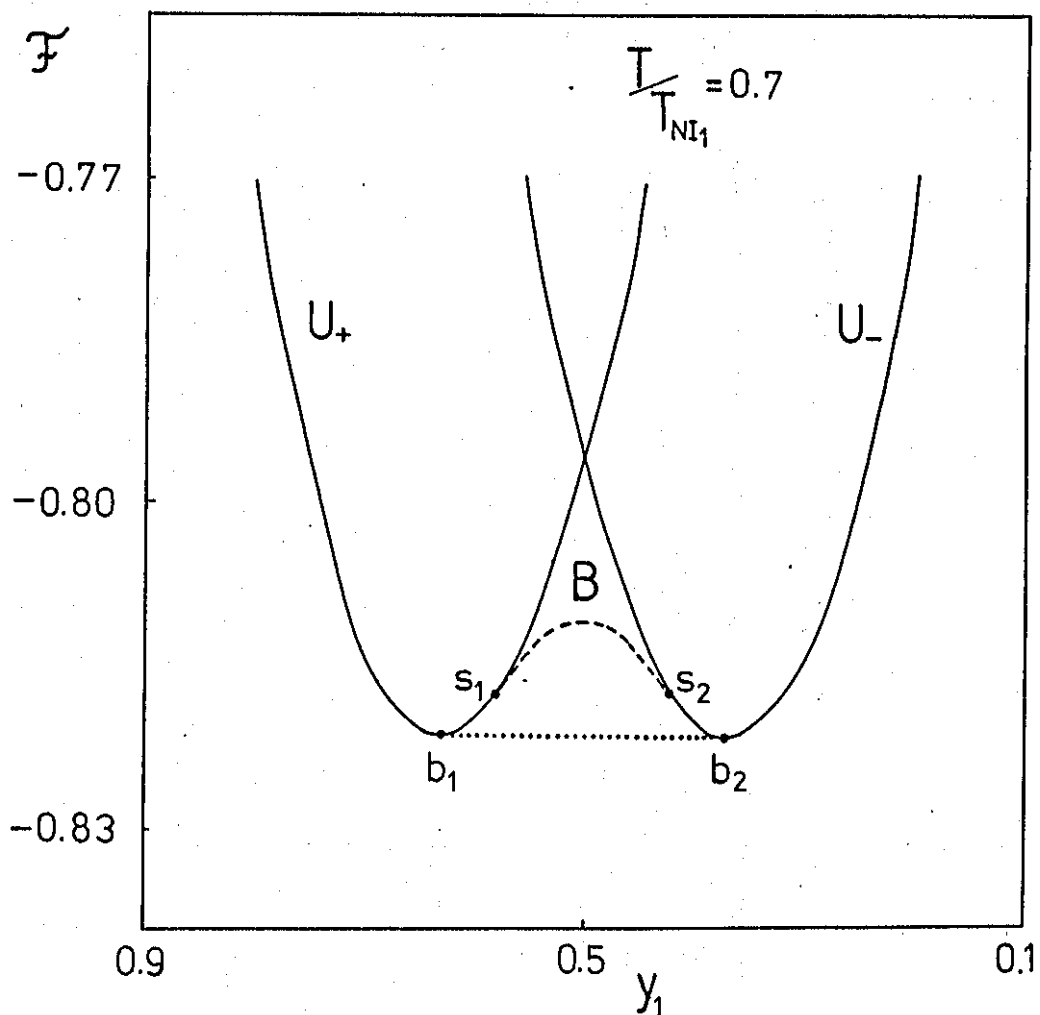


Figure 2.3

Free energy density plotted against  $Y_1$ , the volume fraction of component 1 for mixtures with  $T_{NI1}/T_{NI2} = 1.0$  and  $V_1/V_2 = 1.0$ . Uniaxial solutions are shown with solid lines and the biaxial solution with the dashed line  $s_1 - s_2$ . The double tangent construction joining points  $b_1$  and  $b_2$  shows that the coexistence of the uniaxial phases  $U_+$  and  $U_-$  with composition corresponding to  $b_1$  and  $b_2$  has a lower free energy than the biaxial solution  $B$ . (From Palfy-Muhoray et al. 1985B),

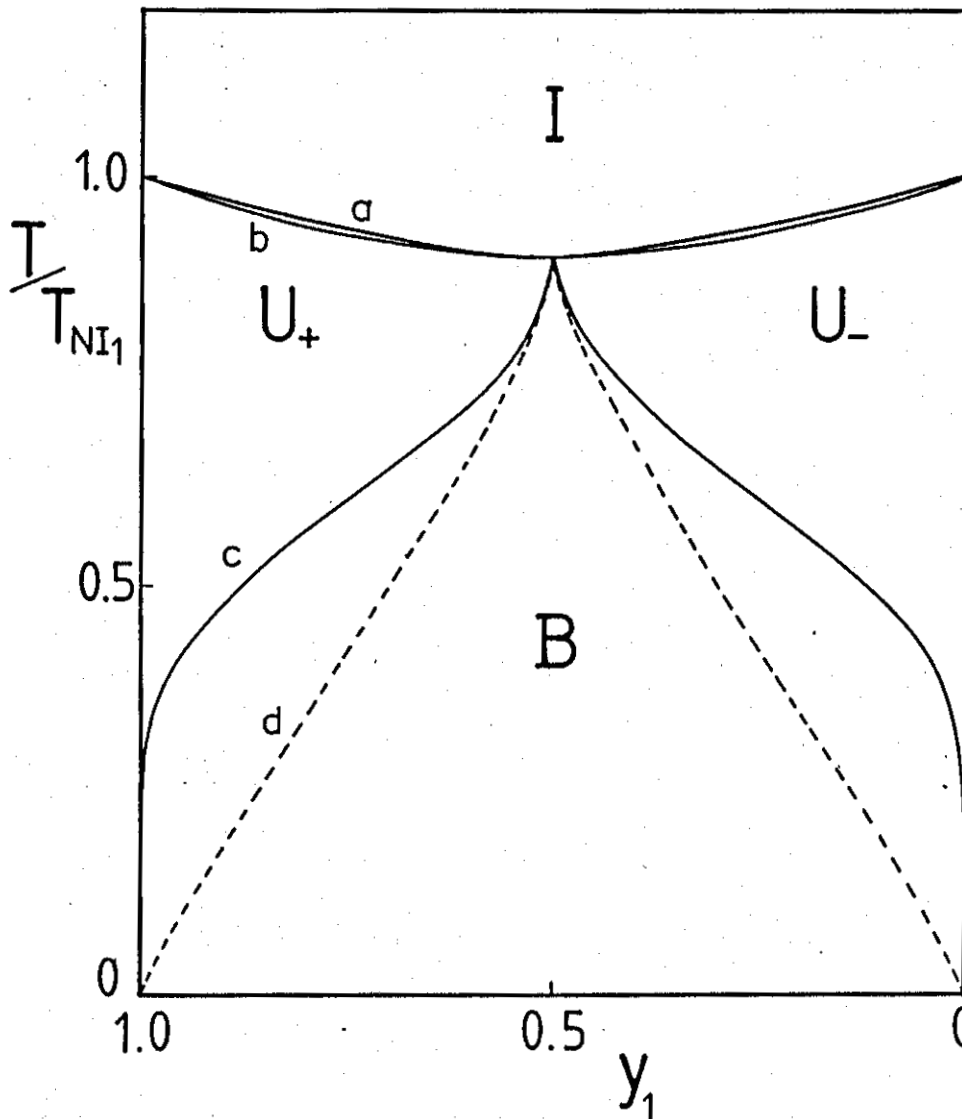


Figure 2.4

Temperature composition phase diagram for mixtures with  $T_{NI1}/T_{NI2} = 1.0$  and  $V_1/V_2 = 1.0$ . The curves a and b are the nematic-isotropic coexistence curves, c is the uniaxial nematic-uniaxial nematic coexistence curve. The biaxial solution exists below d but has a higher free energy as illustrated (From Palfy-Muhoray et al. 1985B).

phases and does not form a biaxial nematic phase.

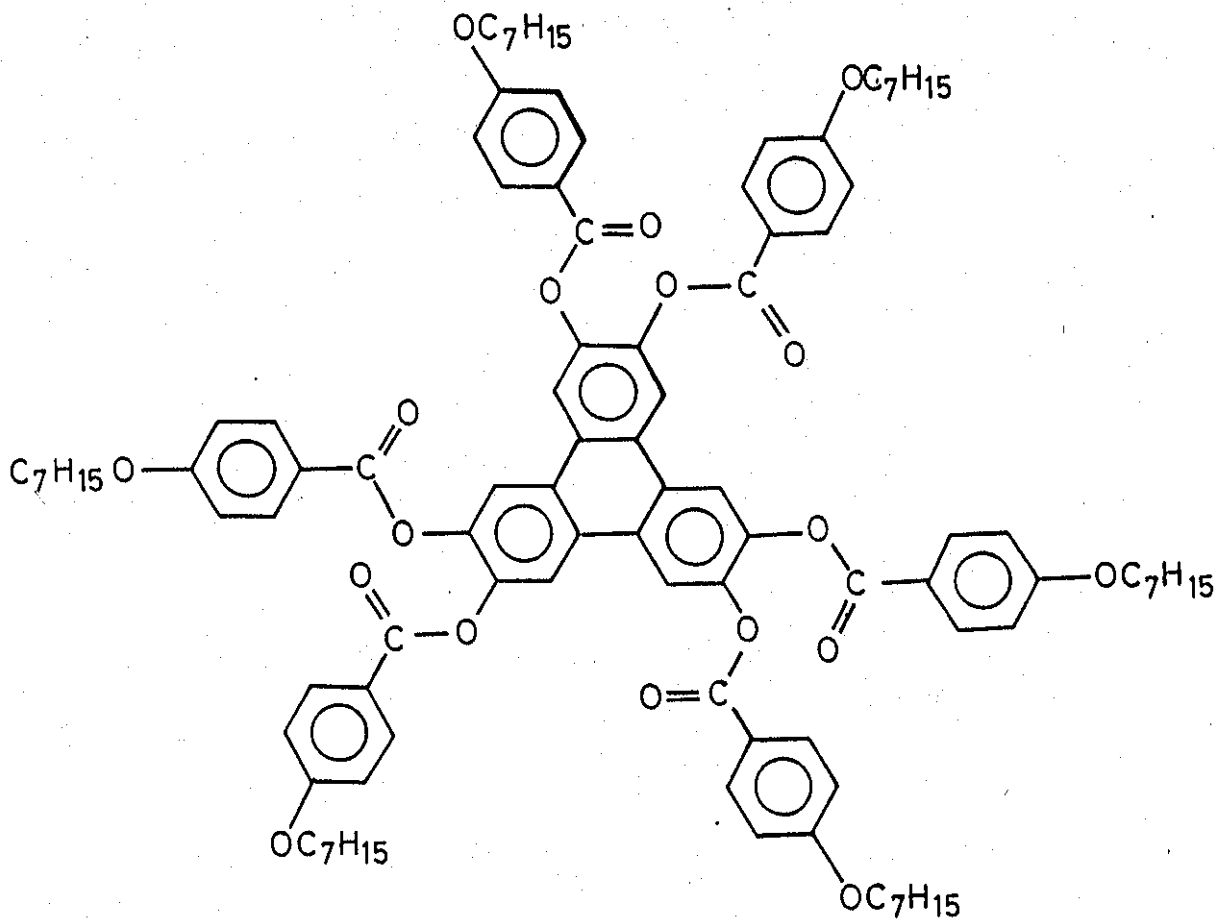
We now present our experimental phase diagrams which support the theoretical model of Palffy-Muhoray et al.

## 2.2 EXPERIMENTAL STUDY OF PHASE DIAGRAMS

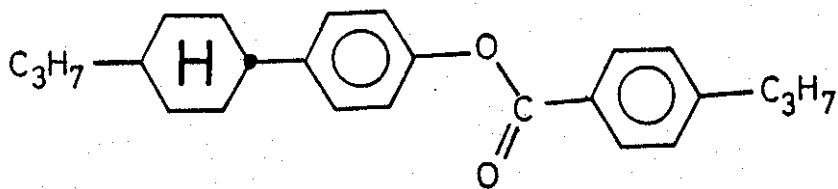
We have studied the detailed phase diagrams of two systems. Both the phase diagrams have been studied only on cooling as the composition does not remain uniform once the mixture is allowed to crystallise.

(a) System I is composed of the rod-like nematogen 4-(trans-4-n-propyl-cyclohexyl)phenyl-4-n-propyl benzoate (3CHP3B) (procured from E.Merck) with a phase sequence  $K$   $89^{\circ}\text{C}$   $N_R$   $186^{\circ}\text{C}$   $I$  and the disc-like nematogen, hexaheptyloxybenzoate of triphenylene ( $C_7\text{OHBT}$ ) (Tinh et al. 1981) with a phase sequence  $K$   $168^{\circ}\text{C}$   $N_D$   $251^{\circ}\text{C}$   $I$ . (This compound was kindly sent to us by Prof. J.Billard.) The structural formulae of the two compounds are as shown in Fig. 2.5. Typical textures exhibited by the  $N_R$  phase of 3CHP3B and  $N_D$  phase of  $C_7\text{OHBT}$  are shown in Fig. 2.6 and Fig.2.7 respectively. 3CHP3B was chosen particularly because it has an I-N transition temperature which is not very much lower than that of  $C_7\text{OHBT}$ , and also the chemical groups in the two compounds are not very different.

The initial observation of the coexistence was made in a contact preparation. Later, quantitative studies were made by making mixtures with specific compositions using a Perkin-Elmer autobalance (Model



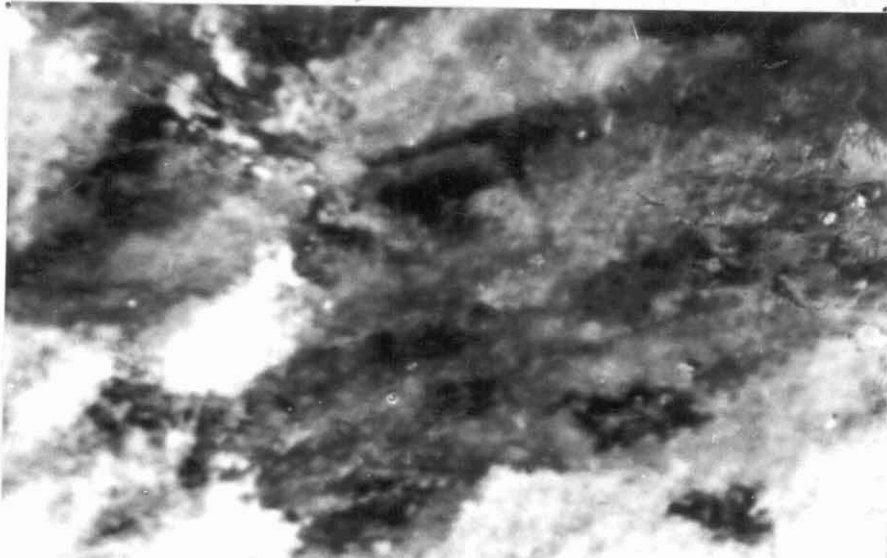
C<sub>7</sub>OHBT



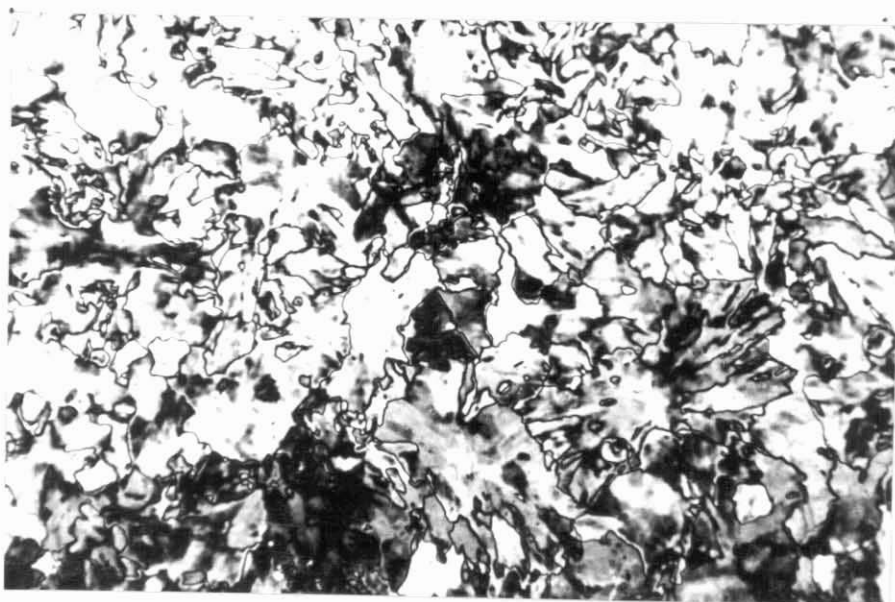
3CHP3B

Figure 2.5

Structural formulae of C<sub>7</sub>OHBT and 3CHP3B.



**Figure 2.6.** The nematic texture of the  $N_R$  phase of 3CHP3B. Crossed linear polarizers (x 450).



**Figure 2.7.** The nematic texture of the  $N_D$  phase of  $C_7OHBT$ . Crossed linear polarisers (x 450)

AD-2). The components were thoroughly mixed in the isotropic phase and the mixture was mounted in the isotropic phase between a slide and coverslip without any spacers. The transition temperatures were noted under a Leitz polarising microscope (Model Ortholux 11-Pol BK) in conjunction with a Mettler hot stage (Model FP 52).

The phase diagram is shown in Fig. 2.8. The I-N transition temperature is depressed very strongly on moving towards the 50:50 mol % region from either end, indicating that the two nematogens are not quite compatible. With less than 5 mol % of C<sub>7</sub>OHBT, as the sample is cooled slowly from the I phase, the N<sub>R</sub> phase starts as droplets, giving rise to a very small coexistence range of I and N<sub>R</sub>. On further cooling the N<sub>R</sub> droplets grow and coalesce to form a uniform nematic phase. With 5 mol % of C<sub>7</sub>OHBT a uniform nematic is obtained, as before, on cooling from the I phase. This has a more or less homeotropic texture (Fig. 2.9a), however on decreasing the temperature further, there is a foggy appearance all over the sample area (Fig. 2.9b) before the sample crystallises.

As the concentration of C<sub>7</sub>OHBT is increased, the N<sub>R</sub> droplets which appear on cooling from the I phase do not coalesce to form a uniform nematic. There is a large range of coexistence of I and N<sub>R</sub> phases. These N<sub>R</sub> droplets have a disclination of strength +1 at the centre (Figs. 2.10 and 2.11) (Dubois-Violette and Parodi 1969).

With further decrease of temperature the N<sub>D</sub> phase starts appearing in the I phase surrounding the N<sub>R</sub> droplets (Fig. 2.12a) result-

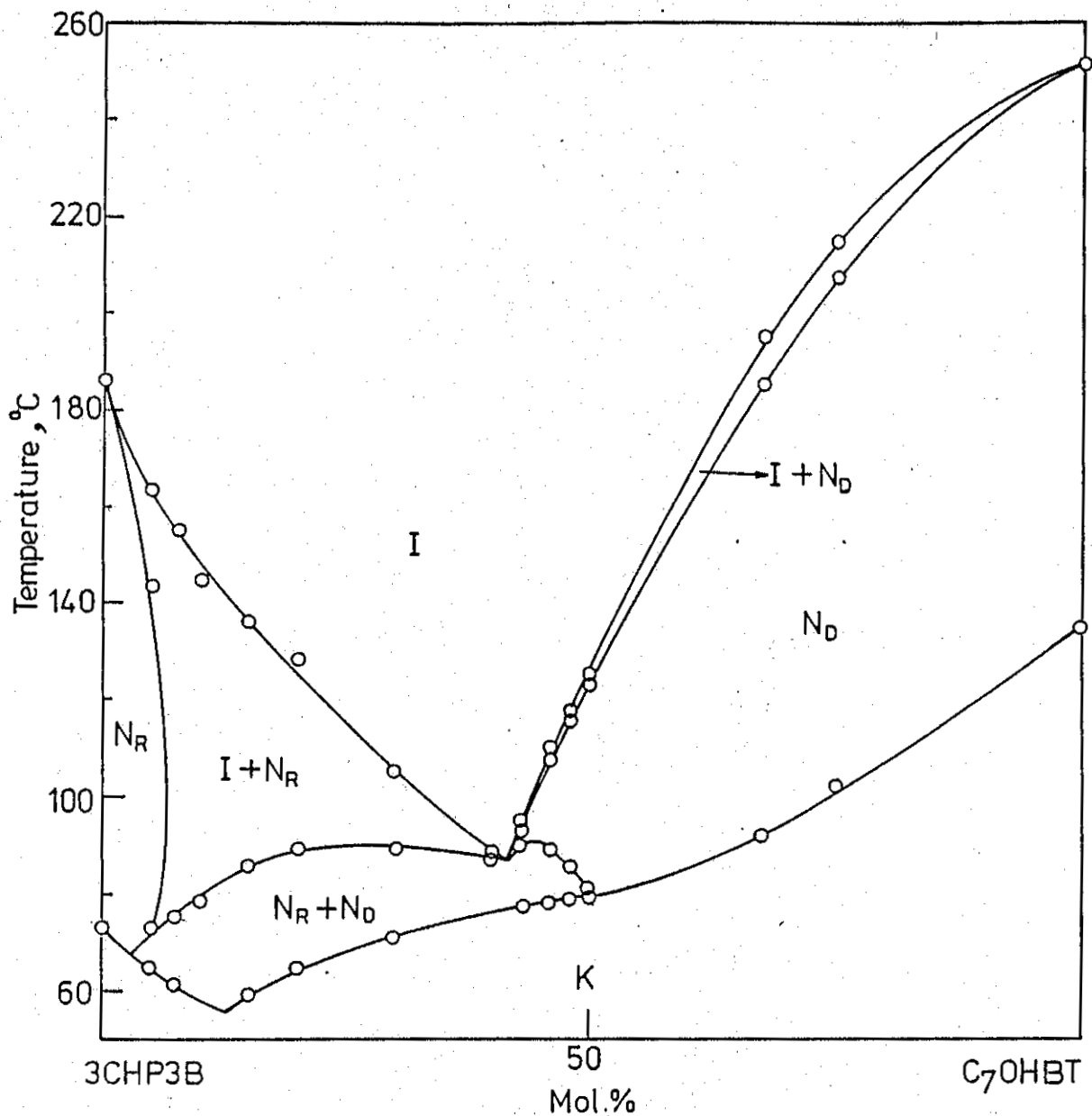
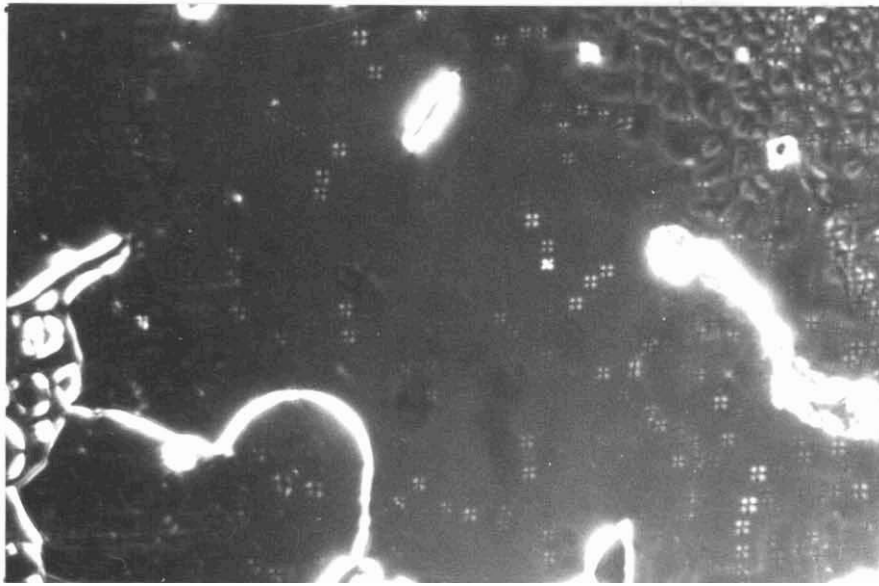
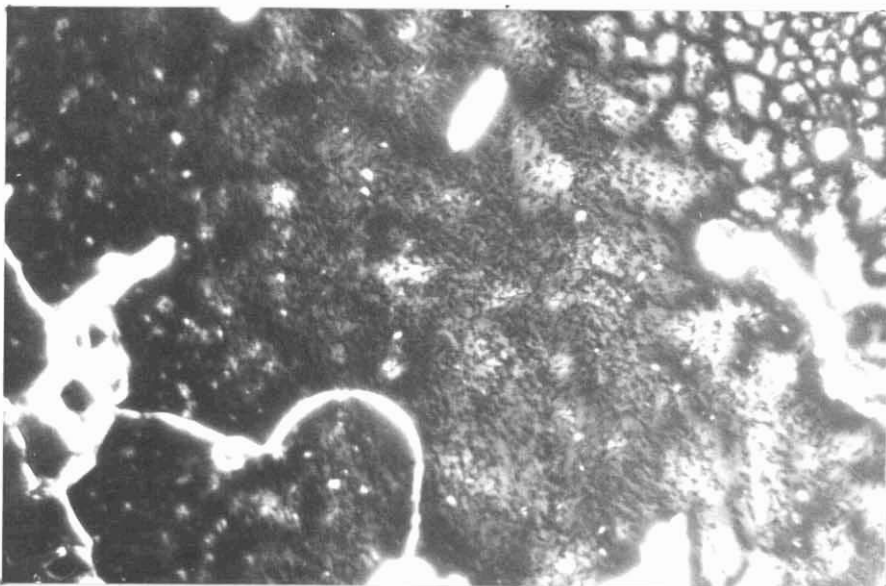


Figure 2.8

Phase diagram of binary mixtures of C<sub>7</sub>OHBT and 3CHP3B (transition temperatures determined on cooling) [System I].



**Figure 2.9a.** Homeotropic texture with 5 mol % of C<sub>7</sub>OHET at 80°C. Crossed linear polarisers (x 450).



**Figure 2.9b.** Same sample area as in Fig. 2.9a at 71.7°C, foggy appearance all over the sample area indicating that a second phase is separating out (x 450).

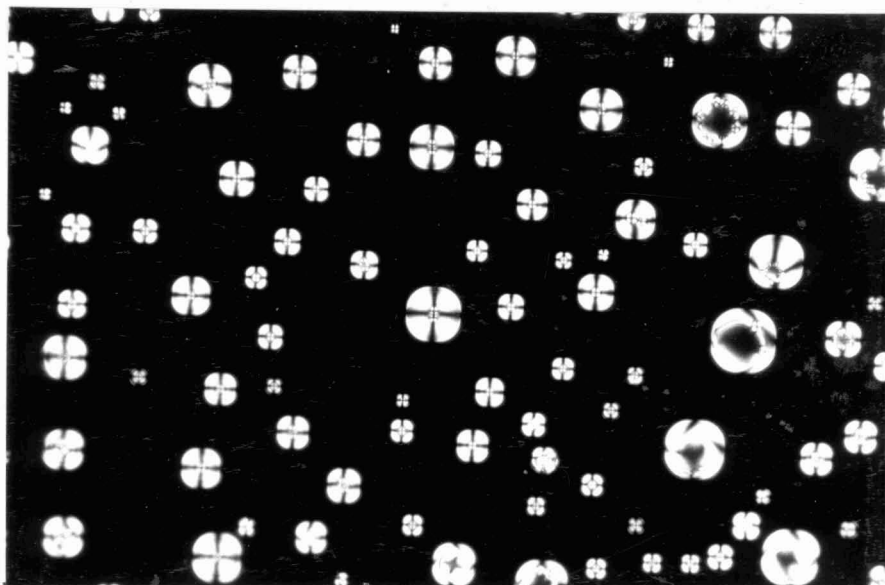


Figure 2.10.  $N_R$  droplets in the I phase each having a point disclination of strength +1 at the centre in a mixture with 30 mol % of  $C_7OHBT$  at  $92^\circ C$ . Crossed linear polarisers (x 450).

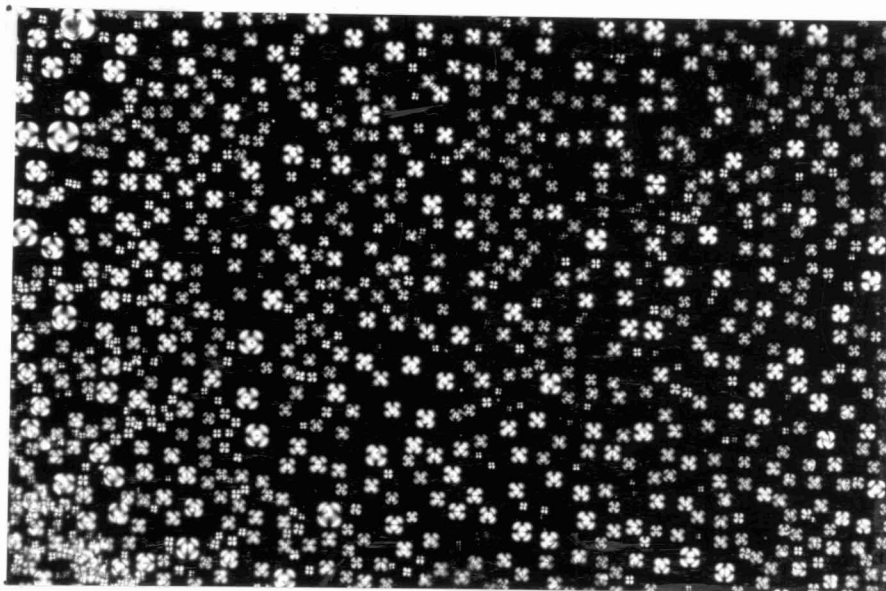
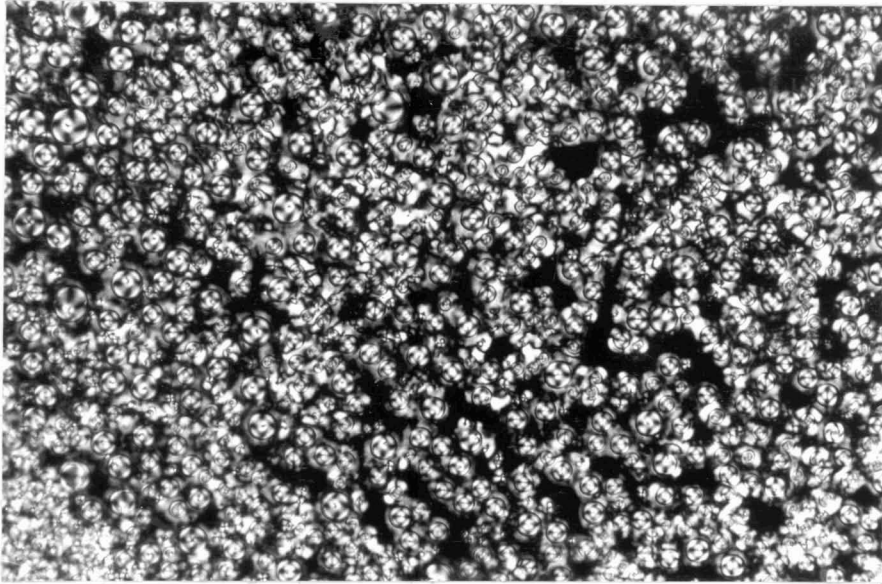
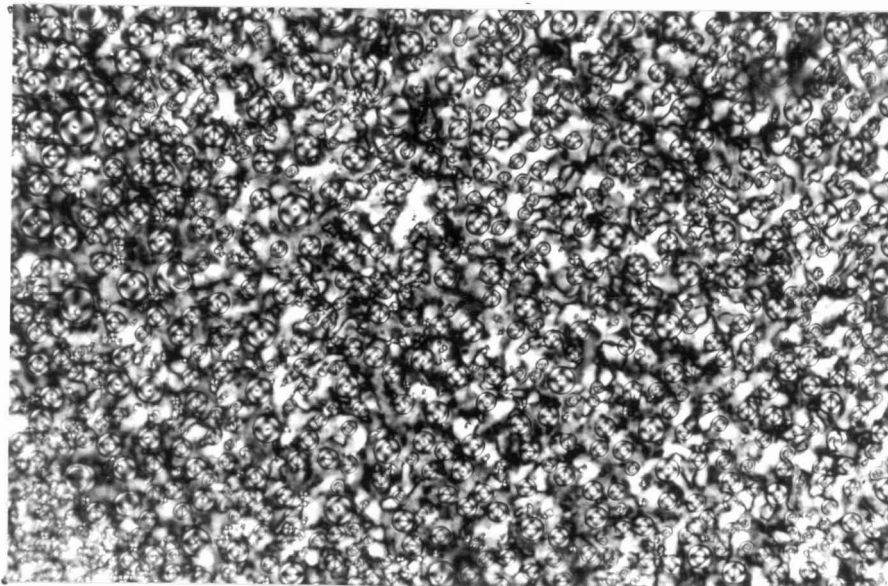


Figure 2.11.  $N_R$  droplets in the I phase in a mixture with 30 mol % of  $C_7OHBT$  at  $91^\circ C$ , with a lower magnification. Crossed linear polarisers (x 215).



**Figure 2.12a.** Same sample area as in Fig. 2.11. The  $N_D$  phase has started appearing in the I phase (x 215).



**Figure 2.12b.** Same sample area as in Fig. 2.12a. Coexistence of  $N_R$  and  $N_D$  phases (x 215).

ing in the coexistence of the  $N_R$  and  $N_D$  phases (Fig. 2.12b). The continuity of the dark brushes across the boundaries between the two nematic phases can be clearly seen by rotating the polarisers (Figs. 2.13a and 2.13b). This coexistence of the two nematic phases remains down to crystallisation.

The phase sequence as indicated in Figs. 2.12a-2.12b is representative of the behaviour of the mixtures having 5 mol % to 41.5 mol % of the discotic compound. The width of the  $I-N_R$  coexistence region decreases with increase in concentration of  $C_7OHBT$  and with 40.0 mol %, the two nematic phases make their appearance in the  $I$  phase almost simultaneously. The  $N_R$  phase starts as tiny droplets, with the  $N_D$  phase immediately surrounding it (Fig. 2.14a). The growth of the two phases continues together as the temperature is maintained (Figs. 2.14b and 2.14c) resulting in the coexistence (Fig. 2.14d).

With further increase in the concentration of  $C_7OHBT$ , the  $N_D$  phase starts appearing first from the  $I$  phase. The coexistence range of the  $I-N_D$  phases in these concentration regions is very small in comparison with the  $I-N_R$  coexistence range in the lower concentration regions of  $C_7OHBT$ . Lowering the temperature results in a uniform  $N_D$  phase (Fig. 2.15a). With further decrease in temperature the  $N_R$  phase starts appearing in the form of tiny droplets which do not grow very large (Fig. 2.15b) and they remain essentially unaltered down to the crystallisation temperature.

This type of coexistence between  $N_D$  and  $N_R$  phases continues

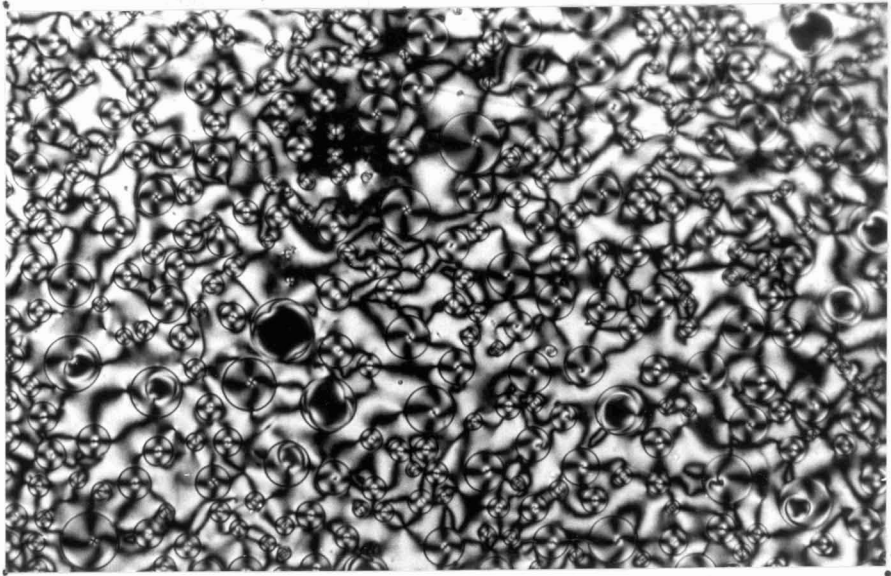


**Figure 2.13a.** Coexistence of  $N_R$  and  $N_D$  phases in a mixture with 30 mol % of  $C_7OHBT$  at  $88^\circ C$  as seen at a higher magnification. Crossed linear polarisers. Note the continuity of dark brushes between the two types of nematics (x 450).

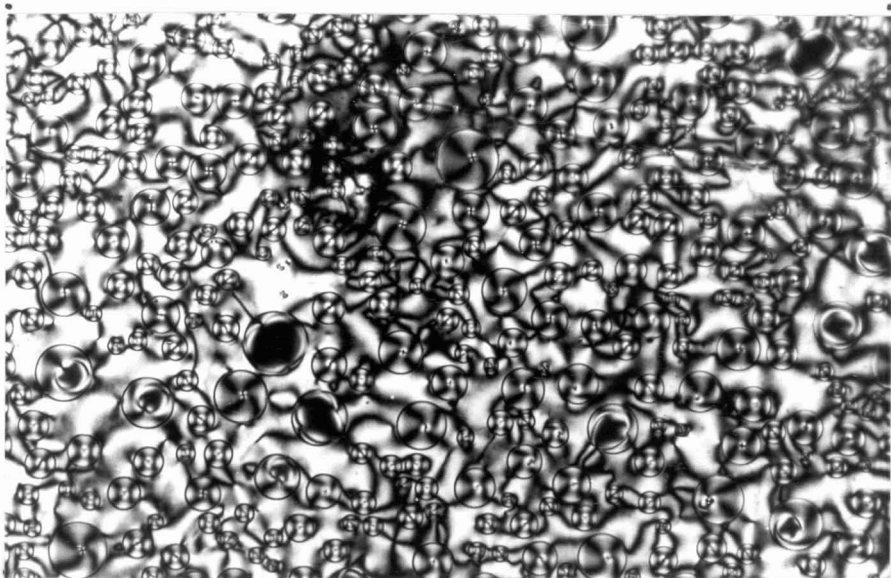


**Figure 2.13b.** Same sample area as in Fig. 2.13a. Polarisers rotated in the clockwise direction by  $45^\circ$  (x 450).

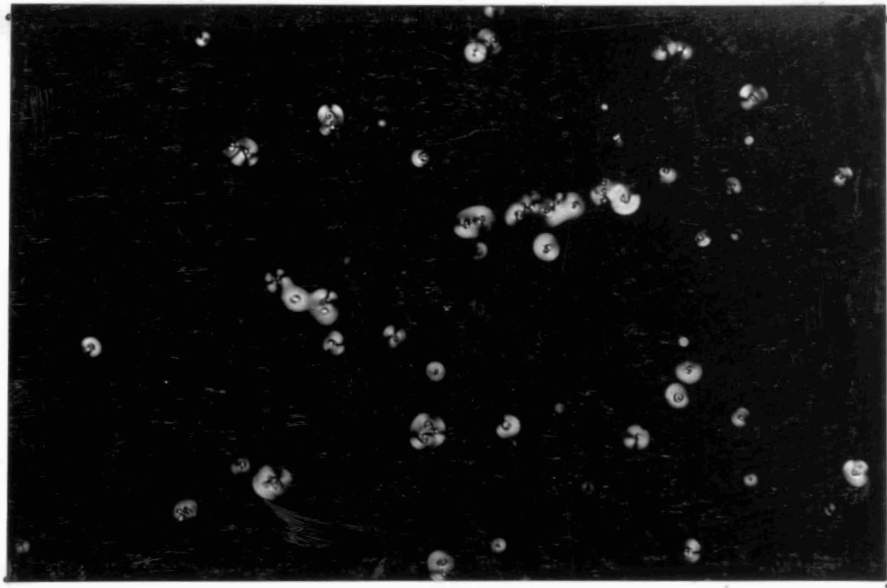


Figure 2.14a.  $N_R$  droplets just starting to form, followed immediately by the  $N_D$  phase in a mixture with 40 mol % of  $C_7OHBT$  at  $88^\circ C$ . Crossed **linear** polarisers (x 450).

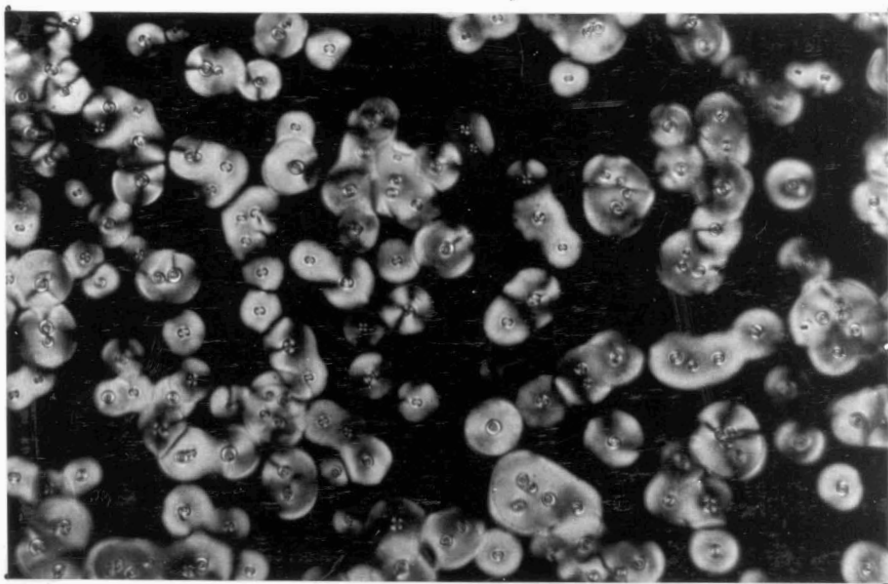


Figure 2.14b. Same sample area as in Fig. 2.14a at a later time. Both the  $N_R$  and  $N_D$  phases are growing (x 450).

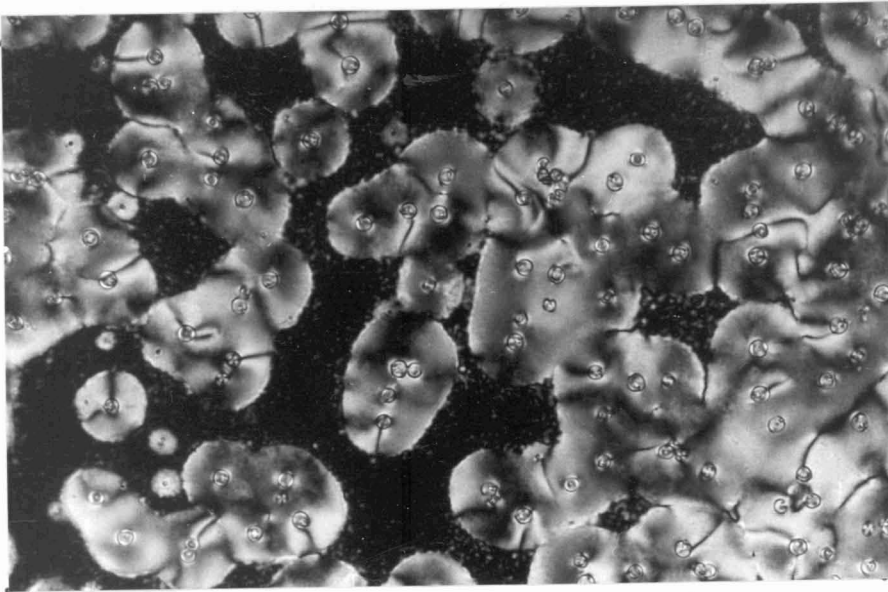


Figure 2.14c. Same sample area as in Fig. 2.14b. There is a further growth of both the  $N_R$  and  $N_D$  phases (x 450).

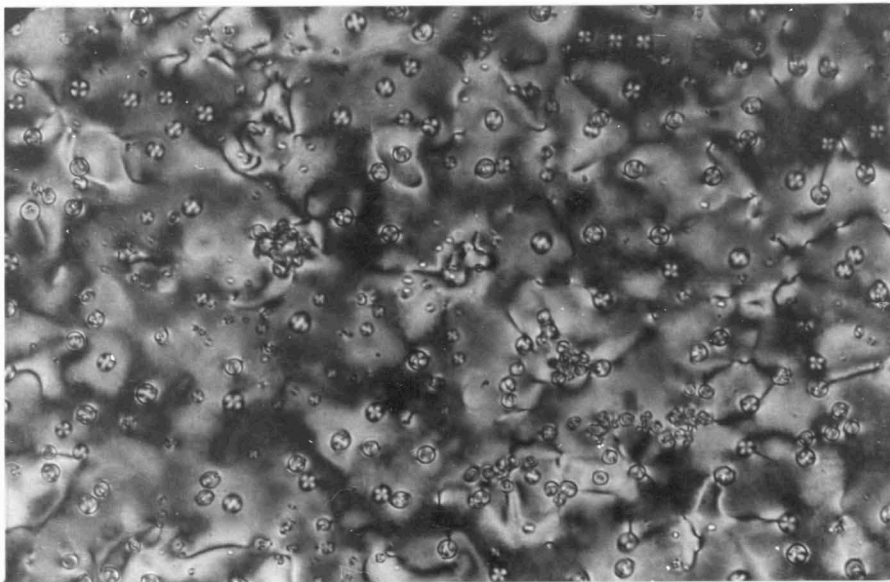
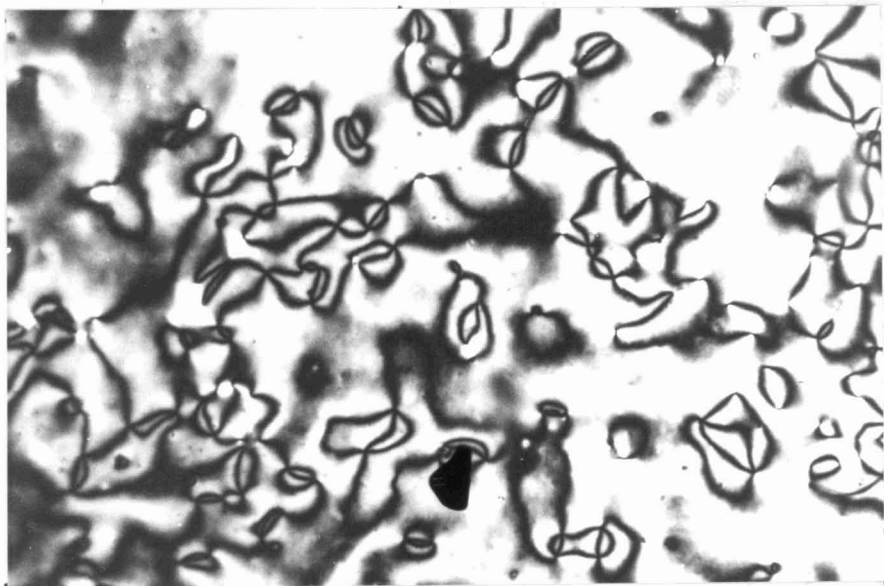
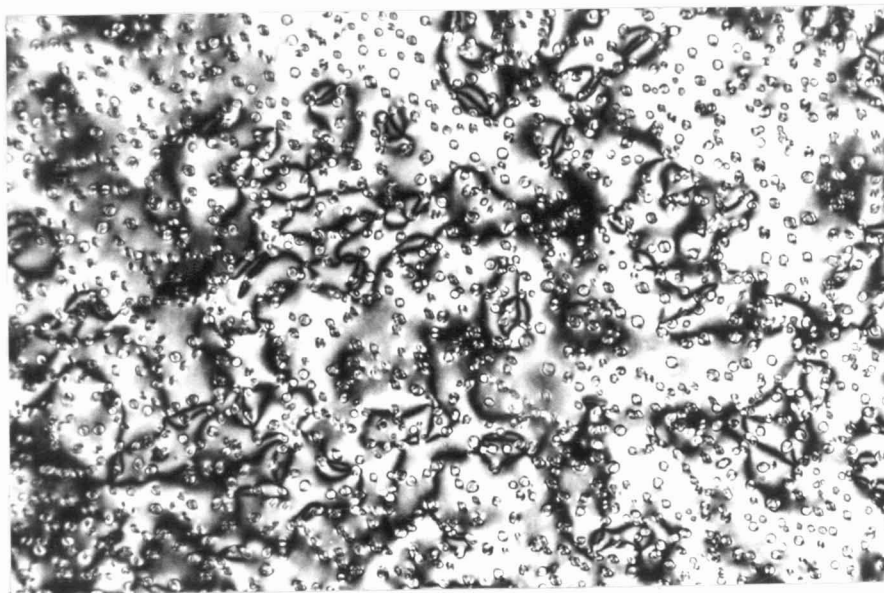


Figure 2.14d. Same sample area as in Fig. 2.14c at 86°C. Coexistence of  $N_R$  and  $N_D$  phases (x 450).



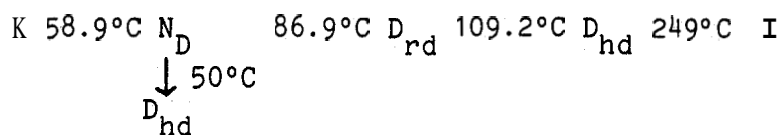
**Figure 2.15a.**  $N_D$  phase in a mixture with 43 mol % of  $C_7OHBT$  at  $95.5^\circ C$ . Crossed linear polarisers (x 450).



**Figure 2.15b.** Same sample area as in Fig. 2.15a after the appearance of the  $N_R$  phase as tiny droplets at  $85^\circ C$ . Coexistence of  $N_R$  and  $N_D$  phases (x 450).

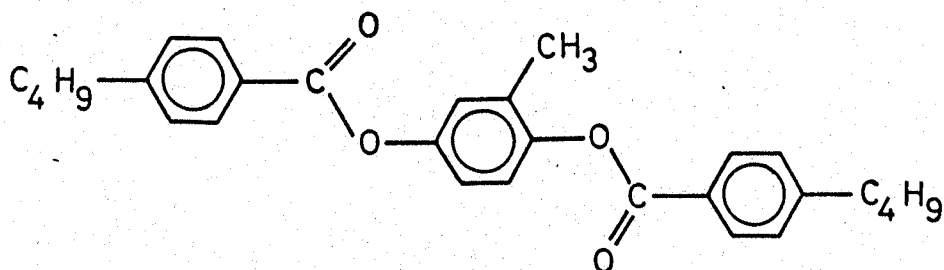
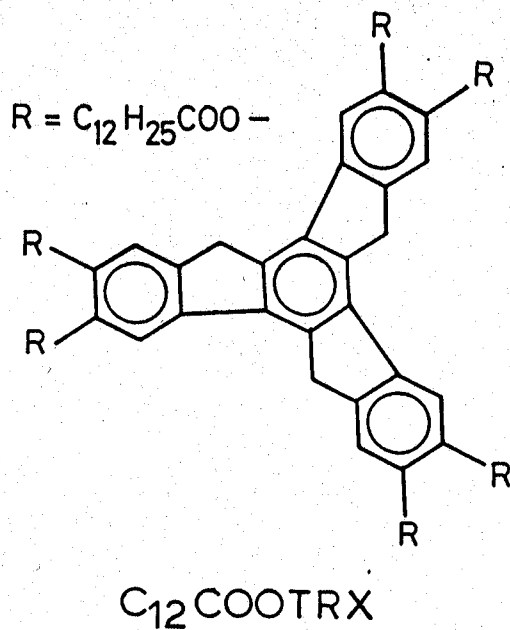
up to 50 mol % of  $C_7OHBT$ . The concentration range over which we have the coexistence of the two nematic phases with the  $N_R$  appearing first from the I phase, is larger than the concentration range in which the  $N_D$  phase appears first. Beyond 50 mol % of  $C_7OHBT$  there is only one type of nematic, viz., the  $N_D$  phase. The  $N_R$  droplets in the coexistence region below 41.5 mol % of  $C_7OHBT$  have an interesting structure when the sample is taken between plates coated with silicon monoxide ( $SiO$ ). This will be discussed later.

b) The rod-like compound used in the second binary system (System II) is 1,4,phenylene (2-methyl) bis(4,n-butyl benzoate) (4PM4B) with the phase sequence K 62.9°C N 140.3°C I, and the discotic compound is hexa-n-dodecyl alkanoyloxy truxene ( $C_{12}COOTRX$ ) (Destrade et al. 1981) (This compound was kindly given to us by Dr. C. Destrade.) The latter exhibits two enantiotropic columnar phases and one monotropic columnar phase in addition to the nematic phase  $N_D$ . The phase sequence of the discotic compound is



where  $D_{rd}$  and  $D_{hd}$  represent the rectangular disordered and hexagonal disordered columnar phases respectively. The  $N_D$  phase in this compound occurs between two columnar phases unlike in  $C_7OHBT$  which has only the nematic ( $N_D$ ) phase.

The structural formulae of the two compounds are shown in Fig. 2.16. The textures exhibited by the  $N_D$  phase, the  $D_{rd}$  and reentrant



4PM4B

Figure 2.16

Structural formulae of  $C_{12}COOTRX$  and 4PM4B.

$D_{hd}$  phases of  $C_{12}$ COOTRX are shown in Figs. 2.17, 2.18 and 2.19 respectively. The phase diagram of the system II is shown in Fig. 2.20a. As in system I there is a strong reduction in the I - N transition temperature, but the  $N_R + N_D$  coexistence region occurs over a very small temperature range which is soon followed by crystallisation.

Interestingly in this system the structure of the  $N_R$  droplets depends on the amount of  $C_{12}$ COOTRX. When the pure rod-like compound is cooled from the I phase there is a very narrow range of coexistence between the I and  $N_R$  phases and the  $N_R$  droplets coalesce very fast to form a uniform nematic phase. However the  $N_R$  droplets that just begin to grow in the I phase seem to have four defects on the N-I interface, indicating that the angle at the interface is  $\sim 45^\circ$  (Madhusudana and Sumathy 1983). Addition of small amounts of  $C_{12}$ COOTRX increases the coexistence range of I and  $N_R$ , and the  $N_R$  droplets with the four defects can be more easily observed. For example, Fig. 2.21 shows the  $N_R$  droplets obtained with 5 mol % of  $C_{12}$ COOTRX. Lowering the temperature results in the appearance of the  $N_D$  phase in the surrounding I phase, but this is soon followed by crystallisation.

With about 10 mol % of  $C_{12}$ COOTRX the  $N_R$  droplets have the bipolar configuration (Fig. 2.22a) indicating a **tangential** boundary condition of the director at the I -  $N_R$  boundary (Dubois-Violette and Parodi 1969). Some smaller droplets in Fig. 2.22a have a dark cross in the centre and are droplets with the bipolar configuration viewed end-on. Decreasing the temperature further results in the



**Figure 2.17.** The N<sub>D</sub> phase of C<sub>12</sub>COOTRX (x 215).

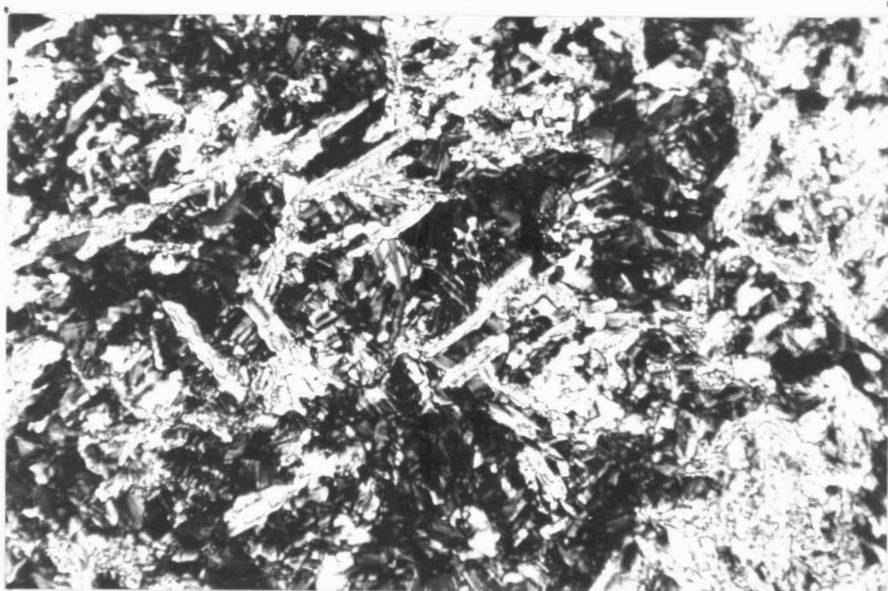


**Figure 2.18.** The D<sub>rd</sub> phase of C<sub>12</sub>COOTRX (x 215).

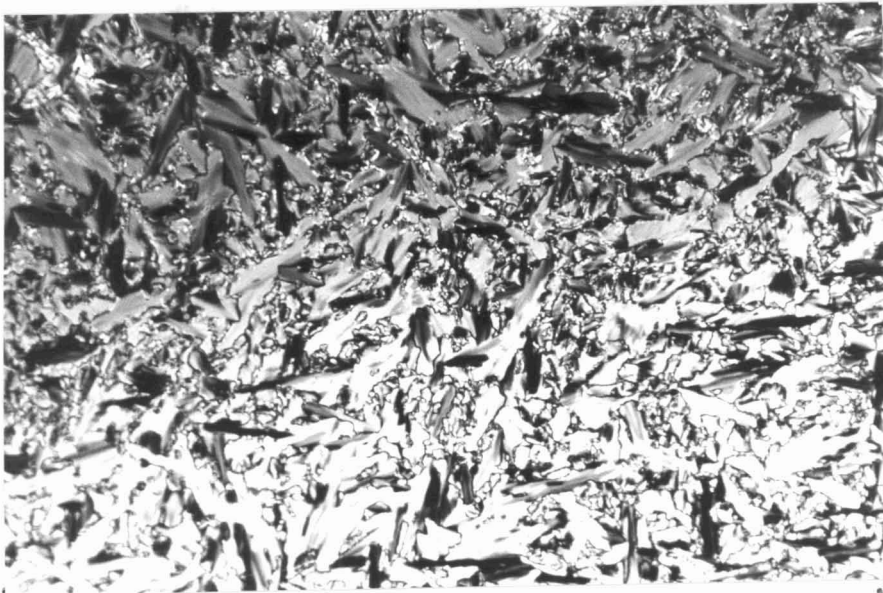


**Figure 2.19.** The reentrant  $D_{hd}$  phase of  $C_{12}$ COOTRX (x 215).

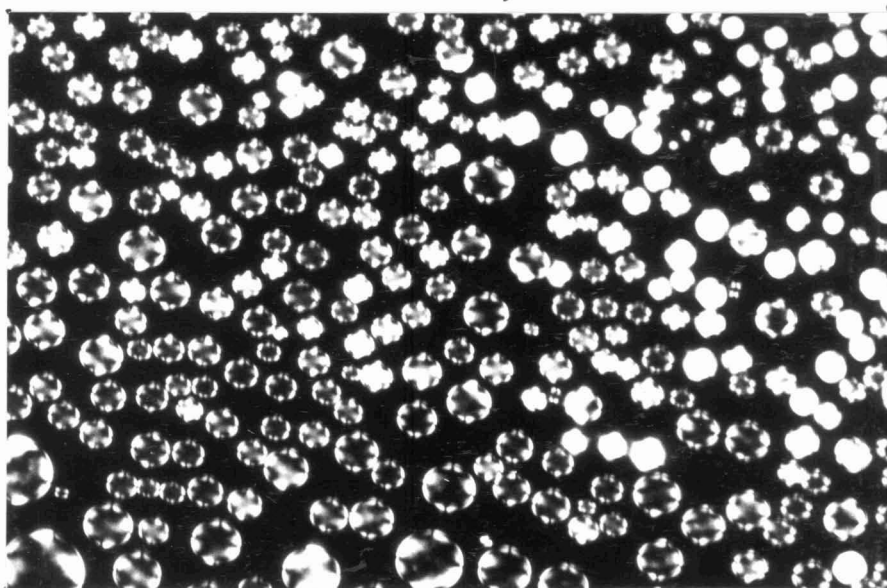


**Figure 2.21.**  $N_R$  droplets in a mixture with 5 mol % of  $C_{12}$ COOTRX at  $127^\circ\text{C}$ , between crossed linear polarisers (x 450).

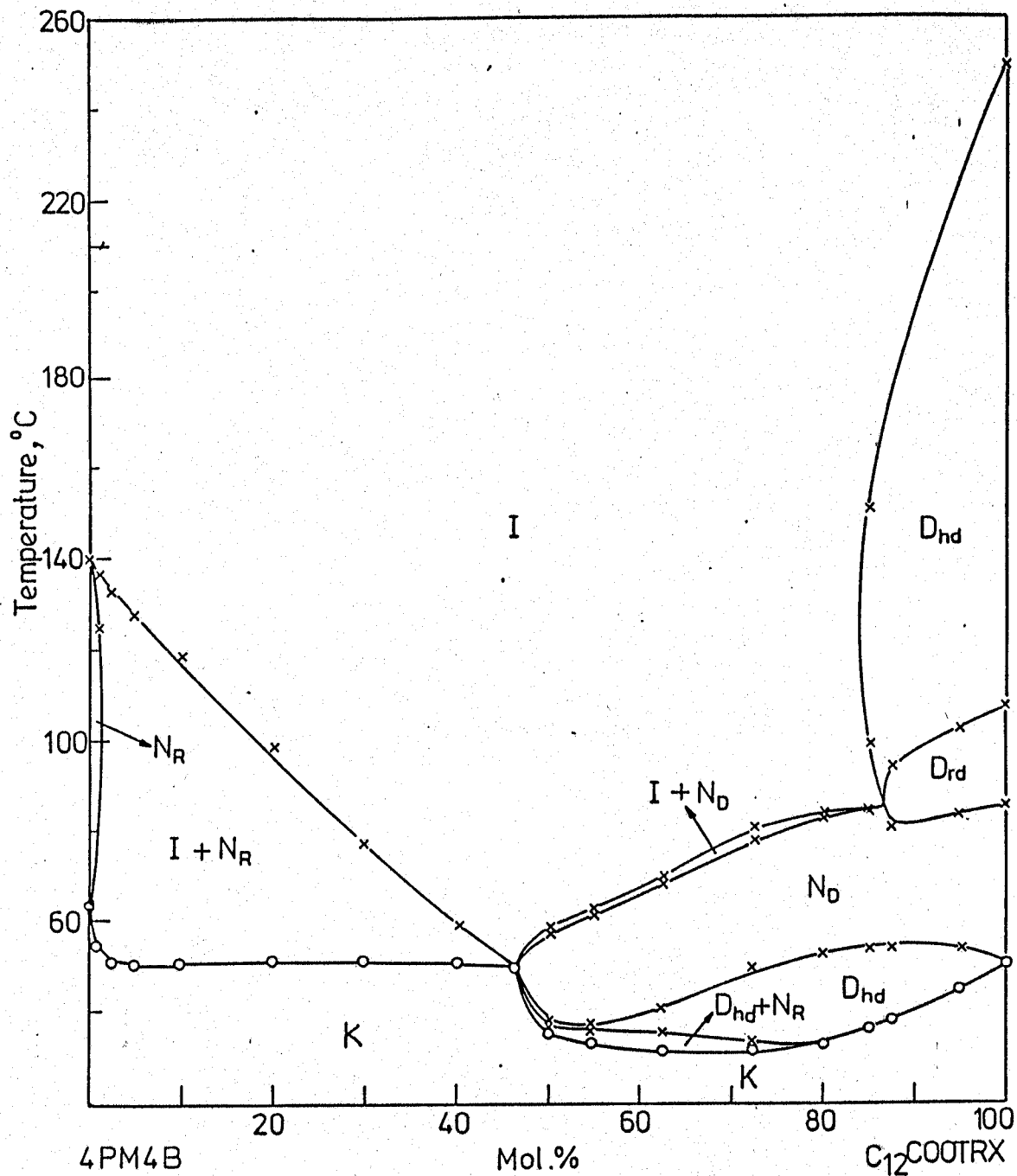
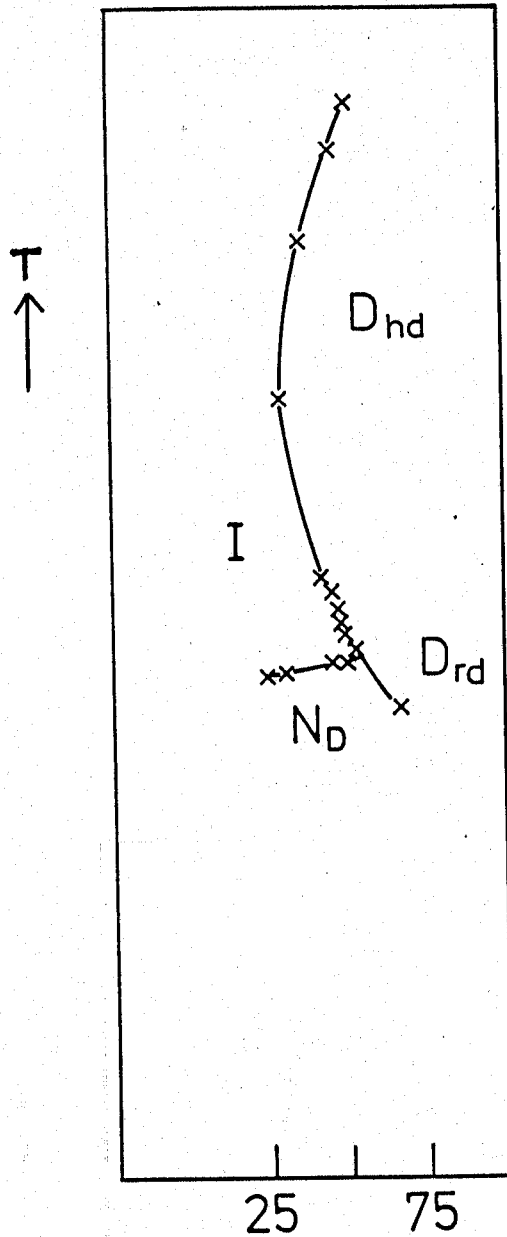


**Figure 2.20a**

Phase diagram of binary mixtures of 4PM4B and C<sub>12</sub>COOTRX (transition temperatures measured on cooling runs) [System II].



Division on the eye piece scale

**Figure 2.20b**

Reentrance of the I phase in System II. The graph has been constructed by noting the transition temperatures at different positions indicated on the x-axis.

appearance of the  $N_D$  phase followed almost immediately by crystallisation (Figs. 2.22b - 2.22d). With further addition of  $C_{12}$ COOTRX, the  $I-N_R$  coexistence range decreases. With about 46.5 mol % the  $N_R$  droplets start in the  $I$  phase followed immediately by the  $N_D$  phase (2.23a). This  $N_D$  phase transforms to the reentrant  $D_{hd}$  phase on further cooling (Fig. 2.23b) to give a coexistence of the  $D_{hd}$  and  $N_R$  phases (Figs. 2.23c-2.23e). This is immediately followed by crystallisation (Fig. 2.23f). All this occurs within a small temperature range and the rapid growth of the stable crystalline phase makes observations difficult.

With further increase in concentration of  $C_{12}$ COOTRX the  $N_D$  phase starts appearing first from the  $I$  phase and covers the entire sample area (Fig. 2.24a). Further decrease of temperature results in the  $D_{hd}$  phase (2.24b) followed by the coexistence of  $D_{hd}$  and  $N_R$  phases before crystallisation. The  $N_R$  droplets which appear on cooling the  $D_{hd}$  phase are not seen distinctly and can be just distinguished on observing the transition very carefully, without any polarisers. Up to 85 mol % of the discotic compound, the  $D_{rd}$  and the higher temperature  $D_{hd}$  phases present in the pure discotic are suppressed.

Around 85 mol % of  $C_{12}$ COOTRX, along with the appearance of the high temperature columnar phases another interesting phase sequence is observed. The  $D_{hd}$  phase which appears from the  $I$  phase remains stable for about 50°C and starts going over to the  $I$  phase on further cooling. This reentrant  $I$  phase is again stable for about

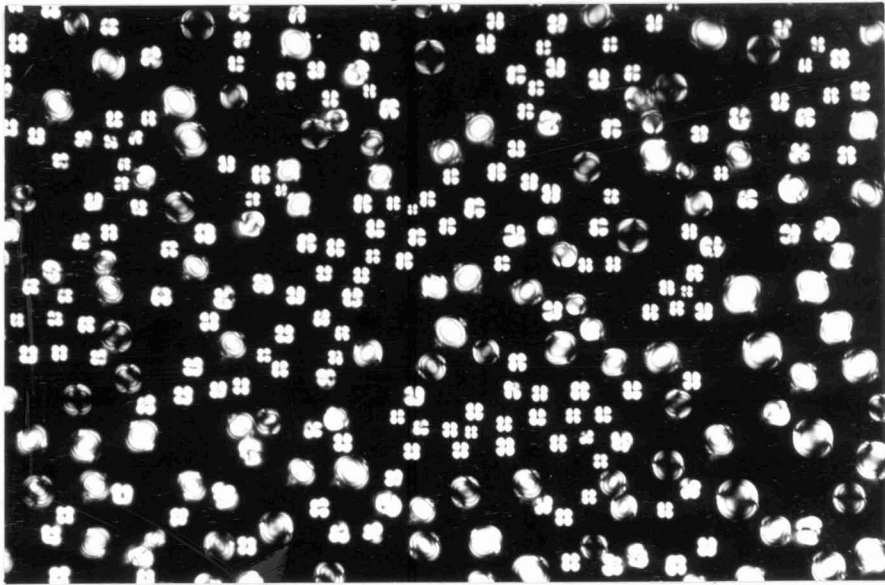


Figure 2.22a.  $N_R$  droplets with a bipolar structure in a mixture with 20 mol % of  $C_{12}COOTRX$  at  $77^\circ C$ , between crossed linear polarisers ( $\times 450$ ).

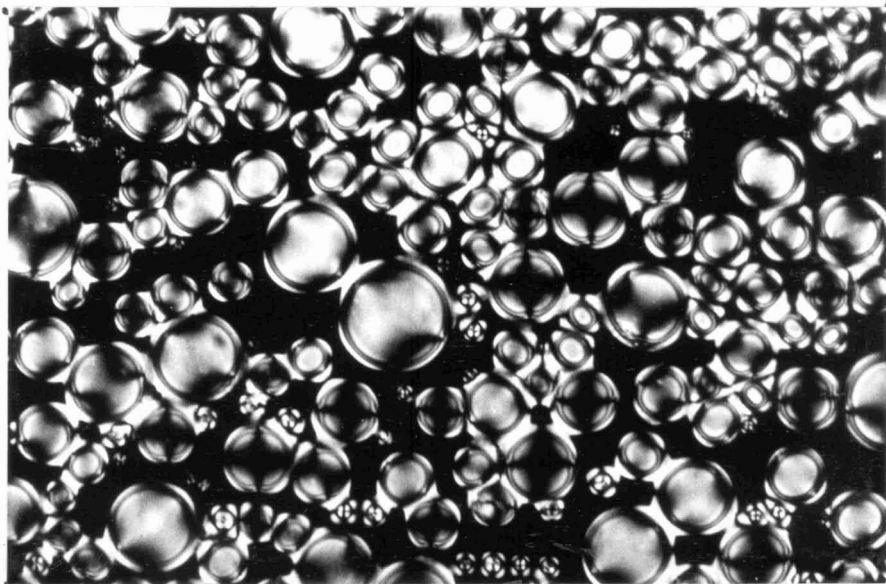
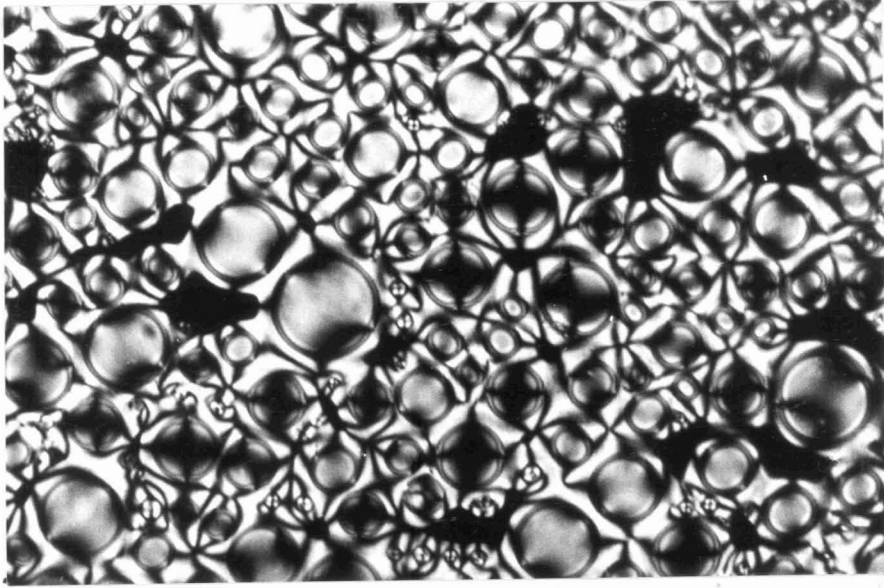
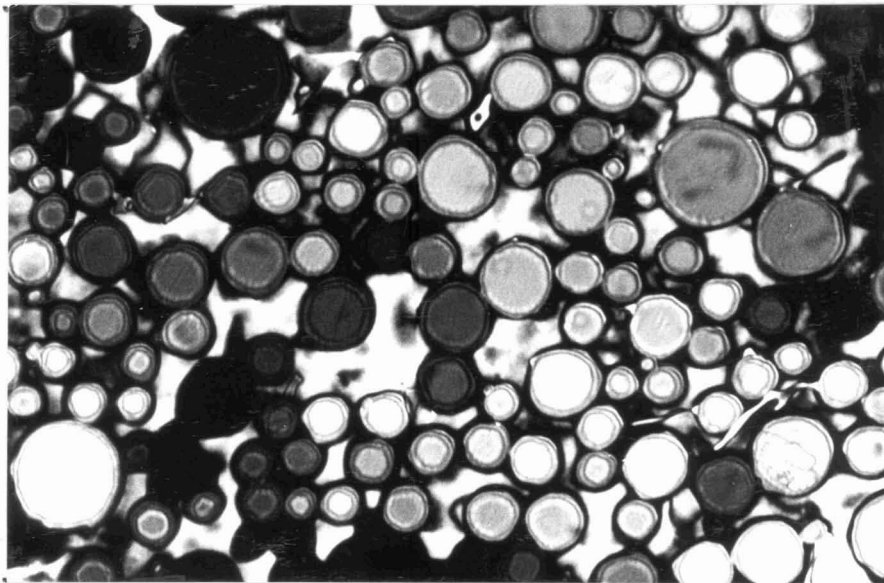


Figure 2.22b. Same sample area as in Fig. 2.22a at  $50.7^\circ C$ ,  $N_R$  droplets have grown larger and  $N_D$  phase has just started appearing in the isotropic phase ( $\times 450$ ).



**Figure 2.222.** Same sample area as in Fig. 2.22b at 50.6°C, growth of  $N_D$  phase almost complete (x 450).



**Figure 2.22d.** Same sample area as in Fig. 2.22c at 50°C after crystallisation of both  $N_R$  and  $N_D$  phases (x 450).

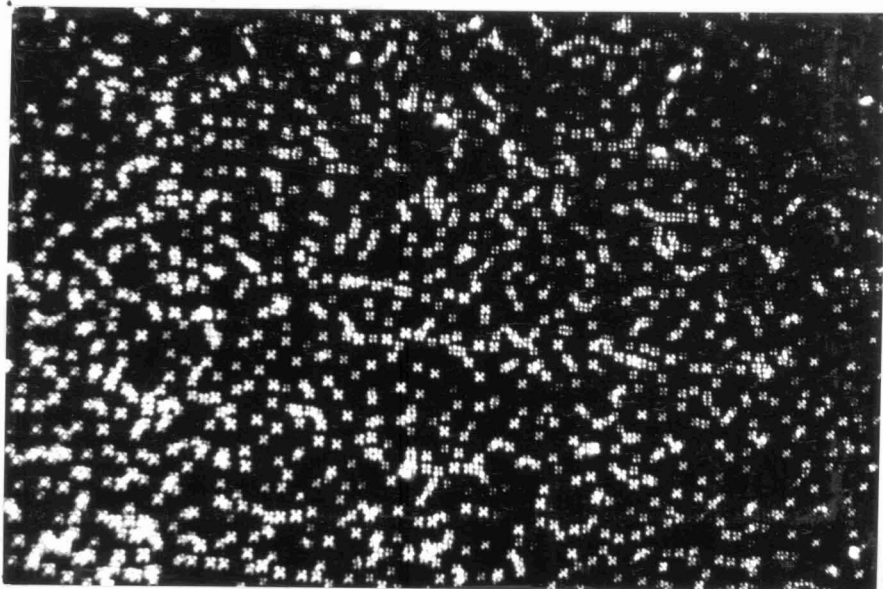


Figure 2.23a.  $N_R$  droplets appearing in the I phase and immediately surrounded by the  $N_D$  phase, in a mixture with 46.5 mol % of  $C_{12}$ COOTRX at  $50.3^\circ\text{C}$ , crossed linear polarisers (x 450).

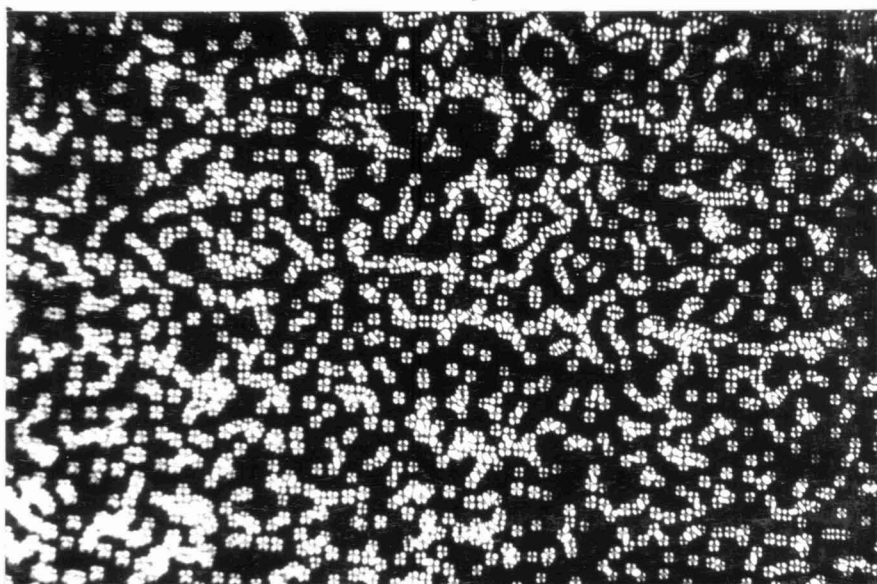


Figure 2.23b. Same sample area as in Fig. 2.23a. The  $N_D$  phase is transforming to the  $D_{nd}$  phase. This photograph has been taken 1/2 a minute after the photograph in Fig.2.23a was taken. (x 450).

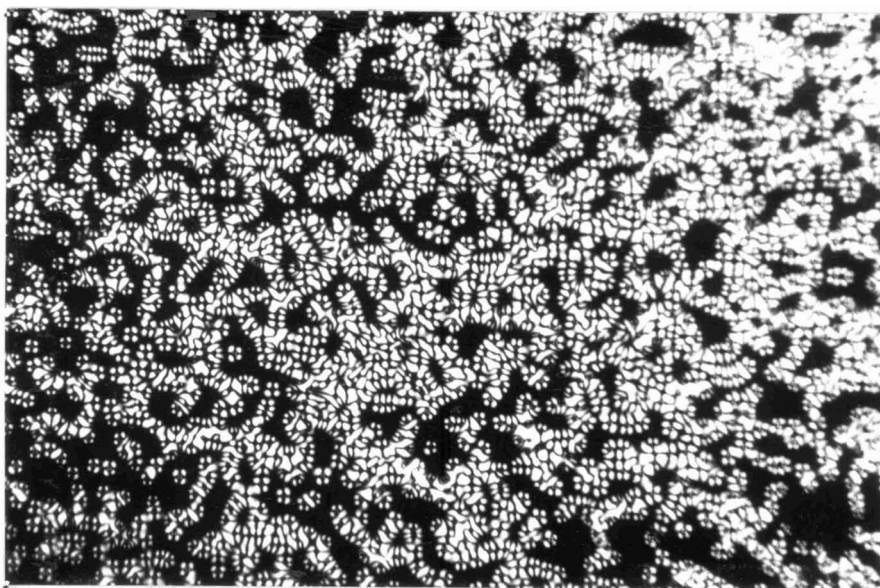


Figure 2.23c. Same sample area as in Fig. 2.23b. Further growth of the  $D_{hd}$  phase can be seen. This photograph has been taken  $1\frac{1}{2}$  minutes after the photograph shown in Fig. 2.23b was taken (x 450).

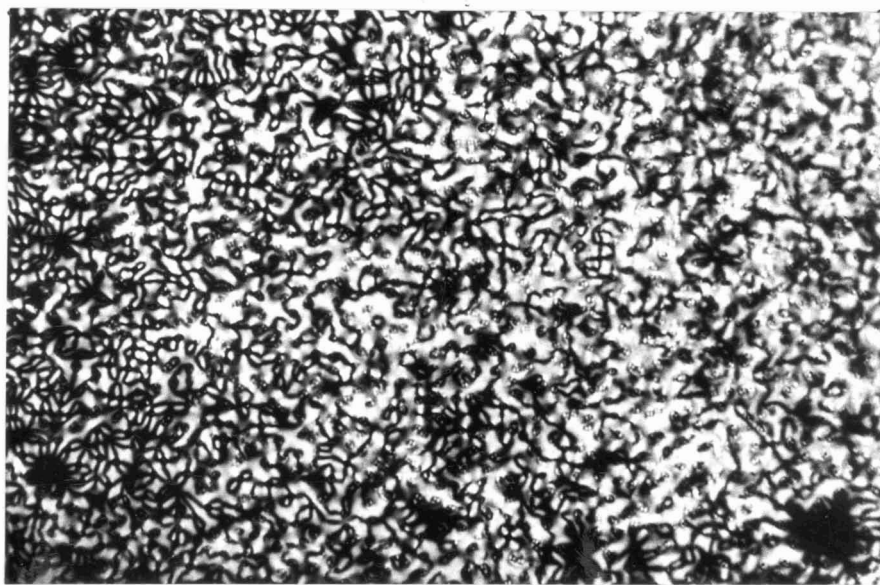


Figure 2.23d. Same sample area as in Fig. 2.23c. Growth of  $D_{hd}$  phase almost complete. This photograph was taken 3 minutes after the photograph shown in Fig. 2.23c was taken (x 450).

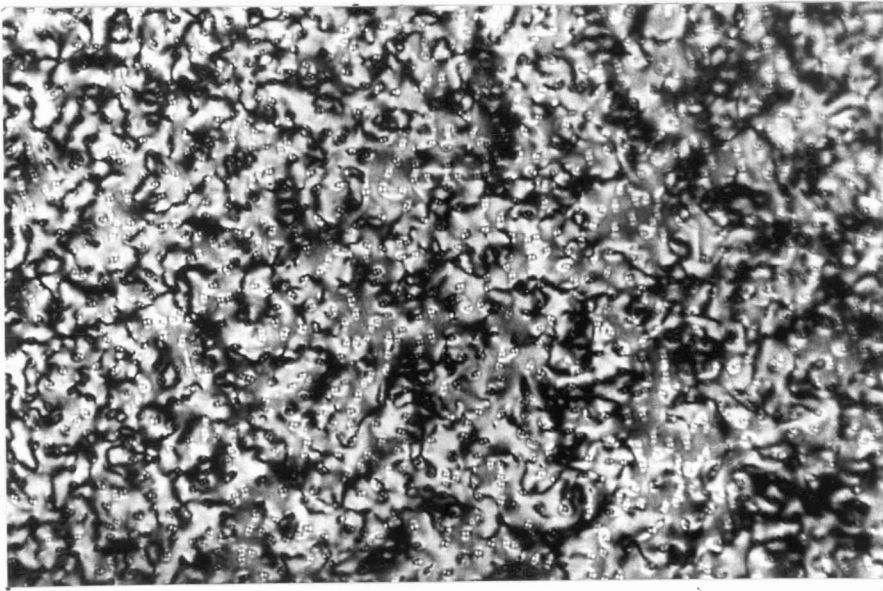
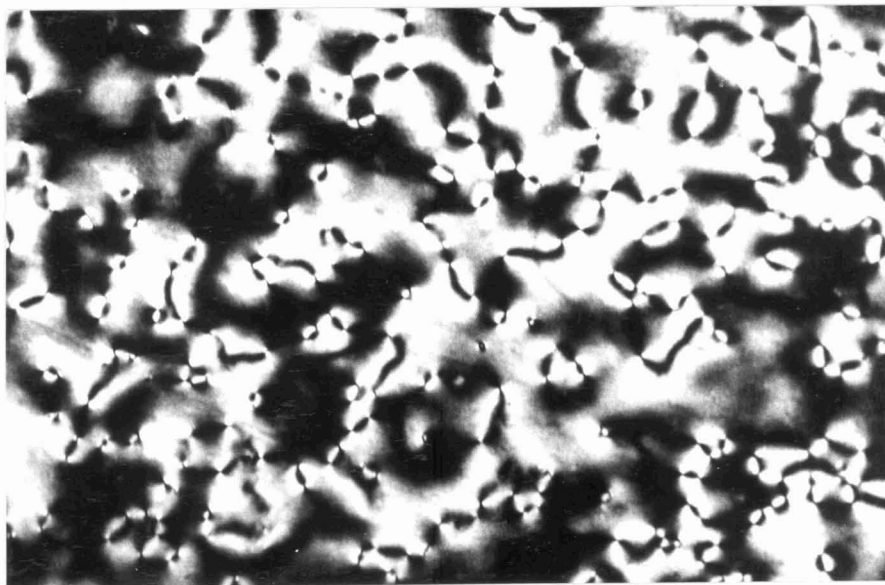


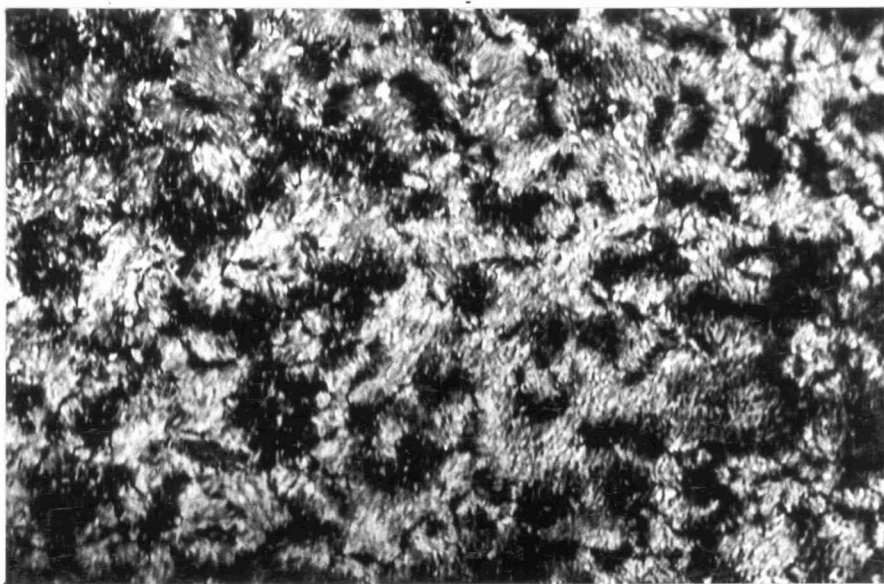
Figure 2.23e. Same sample area as in Fig. 2.23d. Coexistence of  $N_R$  and  $D_{hd}$  phases. This photograph was taken 3 minutes after the photograph shown in Fig. 2.23d was taken (x 450) (see tiny droplets of  $N_R$  still intact).



Figure 2.23f. Same sample area as in Fig. 2.23e after crystallisation of both  $D_{hd}$  and  $N_R$  phases (x 450).



**Figure 2.24a.**  $N_D$  phase in a mixture with 62.5 mol % of  $C_{12}COORX$  at  $42^\circ C$ , crossed linear polarisers (x 450).



**Figure 2.24b.** Same sample area as in Fig. 2.24a at  $35^\circ C$ , the  $N_D$  phase has transformed to the  $D_{hd}$  phase (x 450).

15°C and undergoes a transition to the  $N_D$  phase on further lowering of the temperature. This  $N_D$  phase transforms to the reentrant  $D_{hd}$  phase before crystallisation. This phenomenon of reentrance of the I phase was first observed (Destrade et al. 1982) in a binary mixture of hexa-*n*-tetradecanoyloxy and hexa(4-*n*-dodecyloxy benzoyloxy truxenes, both of which are compounds with disc-like molecules, The reentrance of the I phase obtained in the mixture of system II is only the second such observation.

We have rechecked this reentrance of the I phase in a contact preparation (Fig. 2.20b). The phase sequence could be traced even on heating. This type of phase sequence is however present only for a very small concentration range and further increase in the concentration of the discotic compound leads to transitions similar to those observed with the pure discotic compound.

In this system, in addition to the coexistence of two nematic phases, the coexistence of a columnar and rod-like nematic phase have also been observed. The temperature range over which there is a coexistence of the  $D_{hd}$  and  $N_R$  phases is larger than the temperature range over which there is the coexistence of the  $N_R$  and  $N_D$  phases.

It should however be remarked here that two coexisting nematic phases have been found recently (Casagrande et al. 1982). But this is in a very different kind of system where a side chain polymeric nematogen has been mixed with certain monomeric compounds. The nature of the phase diagram in such systems depends sensitively on the chemi-

cal structure of the monomeric compounds.

Thus our experimental study of the phase diagrams of mixtures of rod-like and disc-like compounds is in good agreement with the prediction of Palffy-Muhoray *et al.* Their theory points out the importance of considering the chemical potentials and leads to the result that two coexisting uniaxial phases have a lower free energy than the biaxial solution. This is the case in the two systems studied by us. The coexistence of the two nematic phases extends over a wider temperature range in System I and the result is therefore clearer in this system. The theory also leads to a nearly symmetrical nematic-nematic coexistence boundary with respect to a composition corresponding to a shallow minimum in the I-N boundary (see Fig. 2 . . . But in System I studied by us the phase diagram has a highly asymmetric shape of this boundary, the coexistence is confined only to compositions rich in the rod-like compound. This is because of the difference in size of the rod-like and disc-like molecules. There is also a large difference in the molecular weight of the two types of compounds. In System I the molecular weight of the disc-like compound is 966 and that of the rod-like compound is only 364. Similarly in System II the molecular weight of the disc-like compound is 1611 whereas that of the rod-like compound is only 444.

In the rod-rich region, the number of discs are few and there are sufficient number of rods to accommodate these discs and give rise to a coexistence of the two types. As the rods are very much

smaller in size, more number of rods are also required to give rise to the coexistence. Therefore in regions richer in the discotic compound, the coexistence of the  $N_R$  and  $N_D$  phases ceases to occur as the number of rods available are not sufficient.

We now discuss the structure of the  $N_R$  droplet in the rod-rich regions' of System I.

### 2.3 STRUCTURE OF THE $N_R$ DROPLETS

Glass plates coated with SiO usually yield a planar alignment of nematic liquid crystals, i.e., the director is parallel to the glass surfaces. As mentioned before when mixtures of system I which exhibit the coexistence of nematic phases are cooled from the I phase, the  $N_R$  droplets appear first and the  $N_D$  phase appears only on further cooling. When such a mixture is taken between SiO coated plates only the  $N_D$  phase which is spread in a continuous manner has a planar alignment and most of the  $N_R$  droplets which are isolated from one another have point defects with strength equal to +1 at the centre of the droplets. Some of the  $N_R$  droplets which have a bigger size are homeotropically aligned (see Fig.2.25a, in the photograph the director of the  $N_D$  phase is aligned parallel to the lower edge). The  $N_D$  phase of  $C_7$ -OHBT is known to give a planar alignment when glass slides with an oblique deposition of SiO are used (Vauchier et al. 1981). The  $N_R$  droplets with a diameter of  $\leq 5 \mu\text{m}$  exhibit the following features when viewed between crossed polarisers.

- a) When the droplet first appears in the **I** phase, the dark brushes that emanate from the centre of the all radial defects with  $s = +1$  are parallel or perpendicular to the polarisers, but with the onset of the  $N_D$  phase the brushes develop a curvature which can be either positive or negative. In Fig. 2.25c the  $N_D$  phase has just started going over to the isotropic phase. Most of the  $N_R$  droplets still have the dark brushes curved whereas in some others which are well surrounded by the **I** phase the dark brushes emerging from the centres of the defects are straight.
- b) When the sample is viewed between crossed circular polarisers 3 spots are visible (Fig. 2.25b). Fig. 2.26a shows a region where almost all the  $N_R$  droplets have a point defect with strength  $+1$  at the centre and Fig. 2.26b shows the same sample area between crossed circular polarisers. One spot corresponds to the  $+1$  defect at the centre. The other two spots are present on the periphery of the  $N_R$  droplets and are diametrically opposite to each other. The line joining these spots makes an angle of about  $10^\circ$  with the normal to the direction in which the  $N_D$  phase is aligned.

The  $N_R$  droplets with a diameter  $\geq 10 \mu\text{m}$  are hornsotropically aligned, i.e., within these droplets the director is normal to the glass surface. There is a brightening on the periphery of these droplets, except in regions parallel or perpendicular to the polarisers

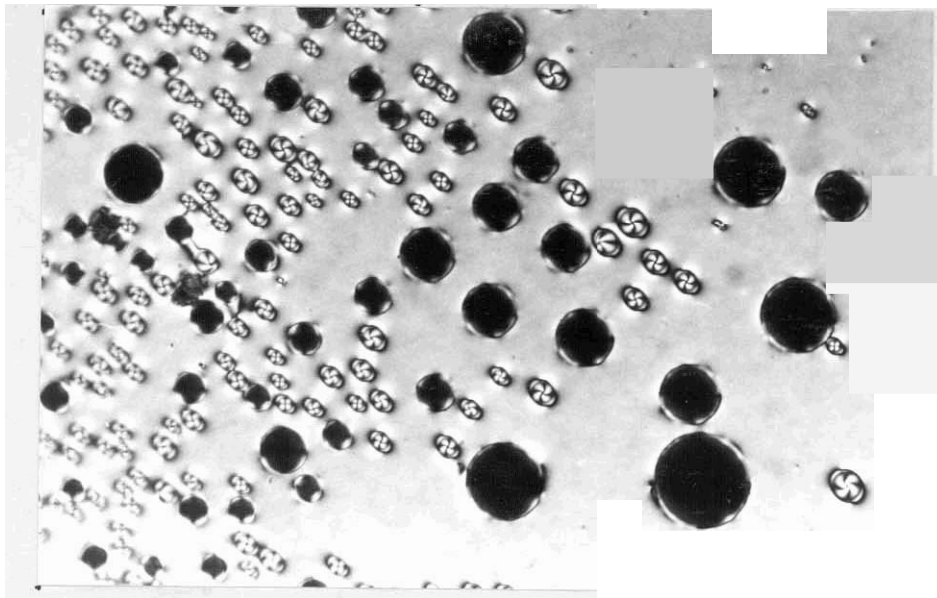


Figure 2.25a. Coexistence of  $N_R$  and  $N_D$  phases in a mixture with 30 mol % of  $C_7OHBT$  at  $88^\circ C$ . Sample taken between  $SiO$  coated plates, crossed linear polarisers ( $\times 450$ ), the brushes inside the  $N_R$  droplets have either positive or negative curvature.

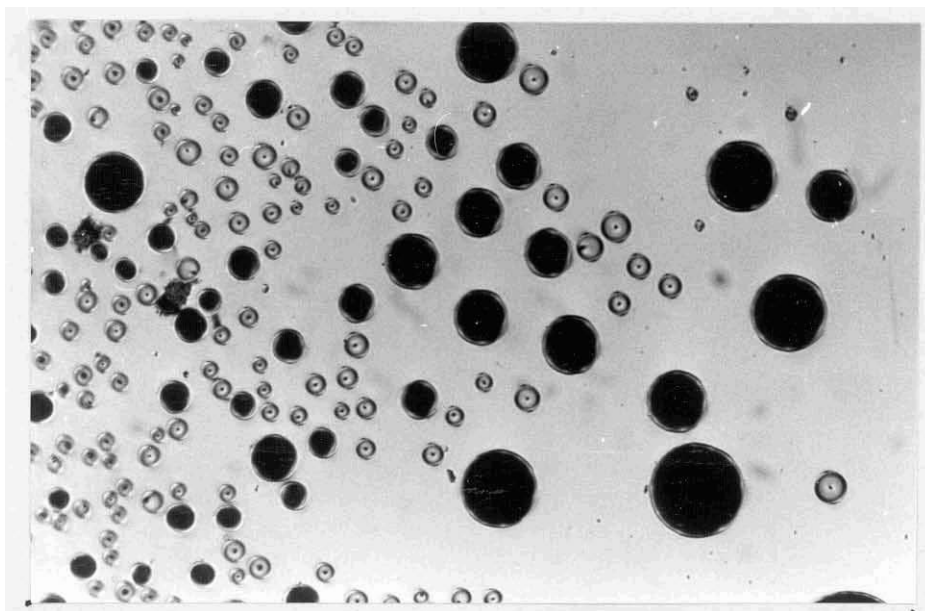


Figure 2.25b. Same sample area as in Fig. 2.25a between crossed circular polarisers ( $\times 450$ ).

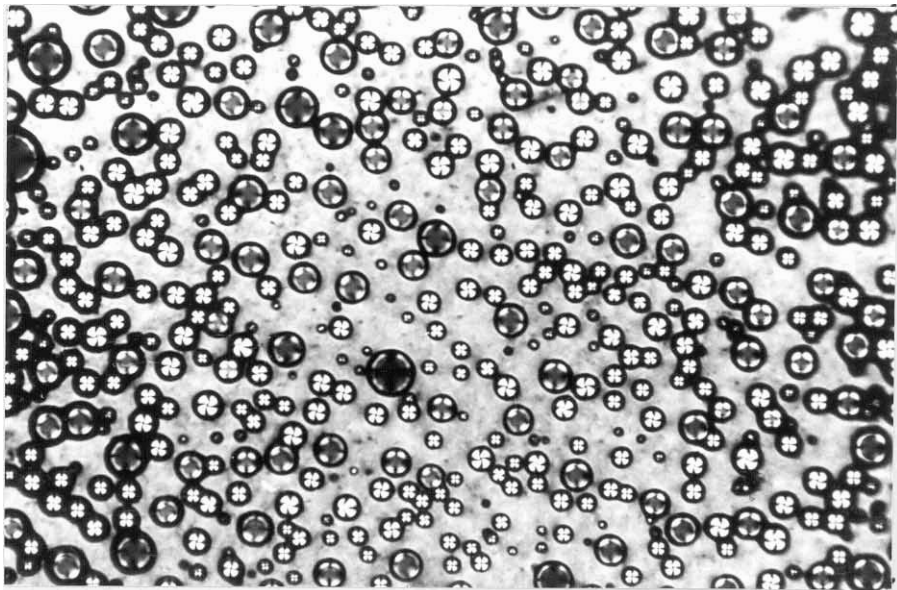


Figure 2.25c.  $N_D$  phase just going over to the I phase at  $91.5^\circ\text{C}$  in a mixture with 30 mol % of  $C_7\text{-OHBT}$ , sample taken between  $\text{SiO}$  coated plates, crossed linear polarisers (x 450).



Figure 2.26a. Coexistence of  $N_R$  and  $N_D$  phases in a mixture with 30 mol% of  $C_7OHBT$  at  $88^\circ C$ , sample taken between  $SiO$  coated plates, crossed linear polarisers (x 450).

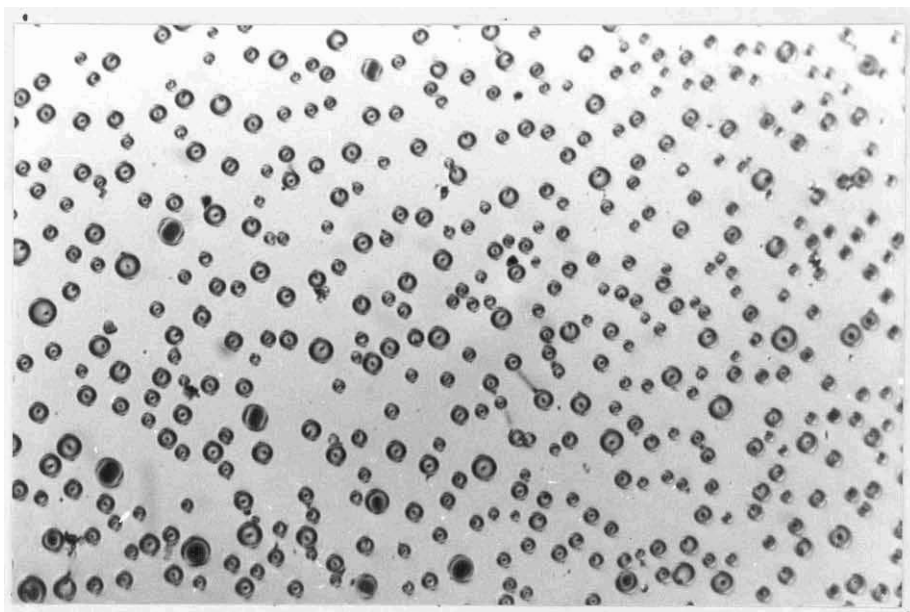


Figure 2.26b. Same sample area as in Fig. 2.26a between crossed circular polarisers (x 450).

(see Fig. 2.25a).

Let us first consider the  $N_R$  droplets with the +1 defects at the centre. The mixtures used in these studies have about 80 mol % of the rod-like compound and the  $N_R$  droplets should have an even higher percentage of the latter compound. The birefringence of the rod-like compound is positive and is higher in magnitude than that of the discotic compound which is  $-0.08$  (Mourey et al. 1982). The sign of optical anisotropy of the  $N_R$  phase can thus be expected to be positive. Observations using a suitable compensator can yield the director distribution within the  $N_R$  droplets. A  $\lambda$  plate was used for this purpose. The quadrants of addition have a blue colour and the quadrants of subtraction have a yellow colour (Hartshorne and Stuart 1934).  $N_R$  droplets with diameter  $\geq 5 \mu\text{m}$  are themselves coloured and identification of the blue or yellow colour is difficult. Therefore smaller droplets with diameter  $\sim 2 \mu\text{m}$  which are essentially colourless were chosen and the quadrants of addition in relation to the direction of the slow axis of the  $\lambda$  plate was noted. The quadrants of addition occurred in a direction parallel to the slow axis of the  $\lambda$  plate indicating that the director is also parallel to the slow axis of the  $\lambda$  plate in these regions. This shows that the director configuration is nearly radial within the  $N_R$  droplets. The curvature of the dark brushes indicates that the director is not strictly normal to the interface, but makes a small angle with the normal. By noting the position of dark brushes with respect to the orientation of the polarisers, the angle at the interface is found

to be approximately  $10^\circ$ . The continuity of dark brushes across the  $N_R - N_D$  interface shows that the director is also continuous across the boundary.

Fig.2.27a shows that topologically the director distortion due to a point defect of strength  $+1$  can be annulled in the far field by a disclination loop or singular ring defect of strength  $-1/2$ , as the director is apolar. Generally in the nematic phase the point defects with strength  $+1$  occur in the bulk of the sample either in a capillary or in spherical droplets with a normal boundary condition. In the samples studied by us, the coexistence of the  $N_R$  and  $N_D$  phases provides a spherical interface between these two phases resulting in a point defect at the centre of the  $N_R$  droplet. As the  $N_D$  phase has a uniform planar alignment the point defect at the centre of the  $N_R$  droplet is compensated by a singular line defect of strength  $s = -1/2$  lying on the periphery of the droplet. Because the droplet is confined between two glass plates and the line defect lies in a plane perpendicular to the plates the singular ring defect appears as two arcs. The two spots seen on the periphery of the droplet with circular polarisers (see Fig.2.25b) correspond to these two arcs of the line defect. The director configuration within and outside the  $N_R$  droplet in a plane parallel to the glass plates and containing the point defect is shown in Fig. 2.27b.

One other instance where a similar configuration has been observed is in the smectic A phase. Trebin (1982) has given such an interpretation of the experimental observations of Perez et al. (1978).

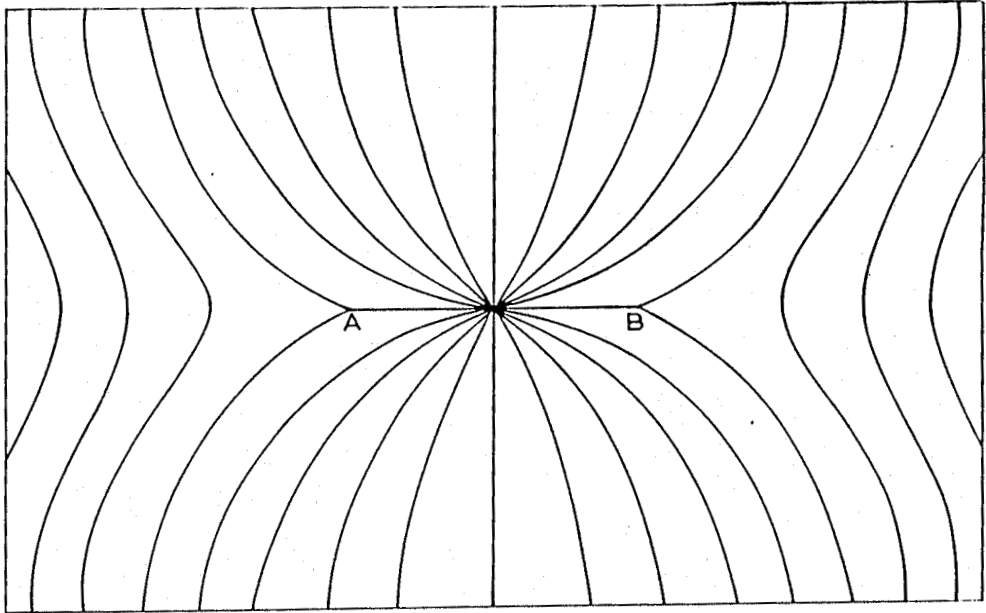
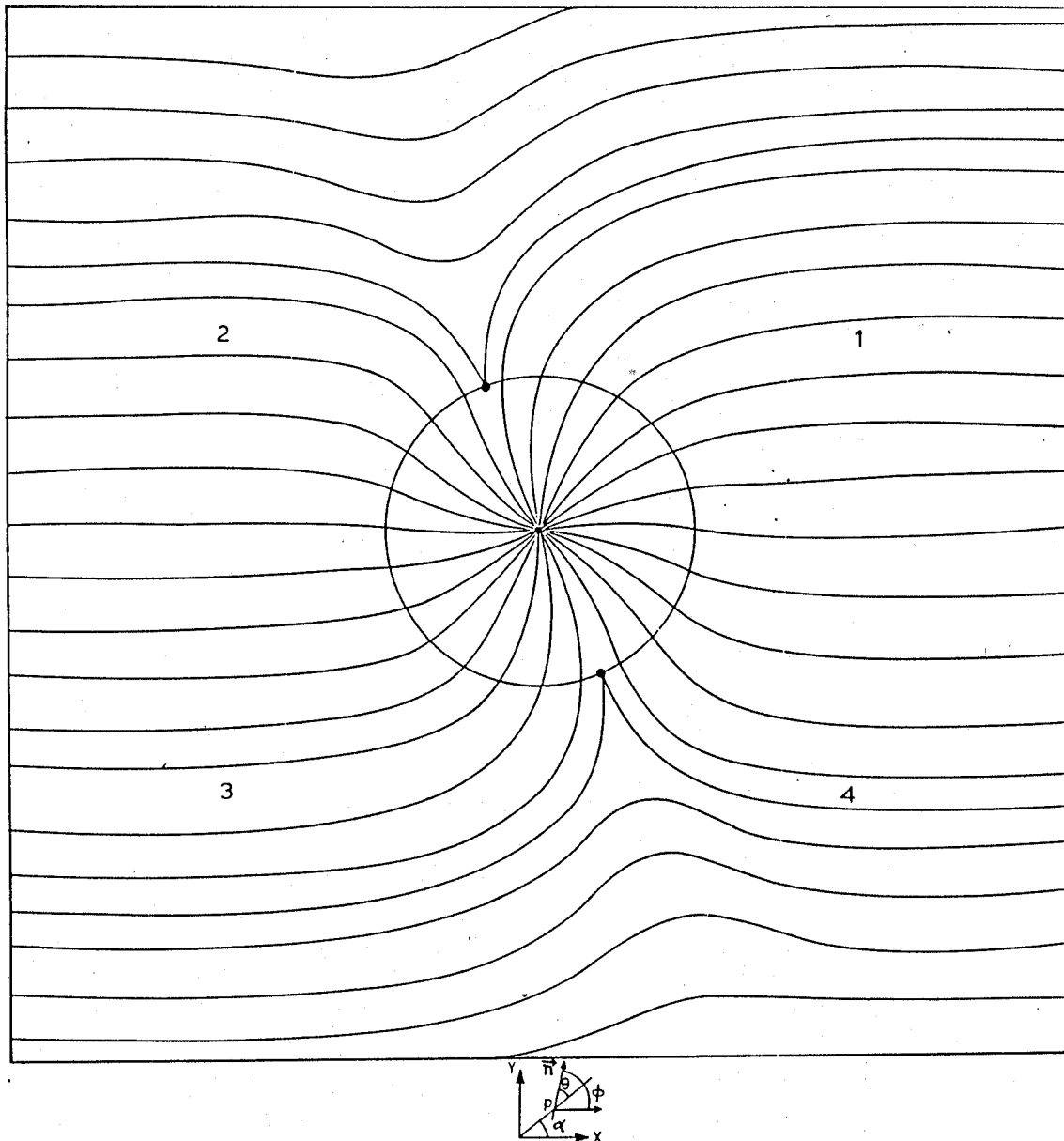


Figure 2.27a

Director distortion around a point defect of strength  $+1$  being annulled by a singular ring of strength  $-1/2$ . The singular ring intersects the paper at points A and B.



**Figure 2.27b**

The director configuration within and outside the  $N_R$  droplet in a plane parallel to the glass plates and containing the point defect, in the samples studied by us.

A hyperbolic point occurring in a smectic A phase which has a layered arrangement can be compensated by a singular ring carrying a topological charge opposite to that of the ring (Fig. 2.28). The layer normal or director field inside the ring has a hyperbolic point defect. The singular ring is necessary outside it in order to maintain the planar layered arrangement in which the layer normal or the director field is uniform.

This is similar to the samples studied by us where the point defect in the  $N_R$  droplet is compensated by a singular ring because the  $N_D$  phase has an overall planar alignment. Ours is the first observation of a singular ring compensating a point defect in a nematic sample. More recently Lavrentovich and Terentev (1986) have found that, in a nematic spherical droplet suspended in an isotropic matrix of glycerin and lecithin, a change in temperature causes a transformation from a radial point defect to a hyperbolic point defect. But in this case it is accompanied by the formation of a non-singular ring disclination. This transition is due to temperature induced changes in the Frank elastic constants.

The dark brushes that emerge from the line defects with  $s = -1/2$ , and present just outside the  $N_R$  droplets, can lie in different regions depending on the orientation of the polarisers.

Let the  $N_D$  phase have an overall planar alignment along the x-axis (see Fig. 2.27b) and let  $\alpha$  be the angle made by the radius vector at any point P outside the droplet with the x-axis,  $\theta$  the

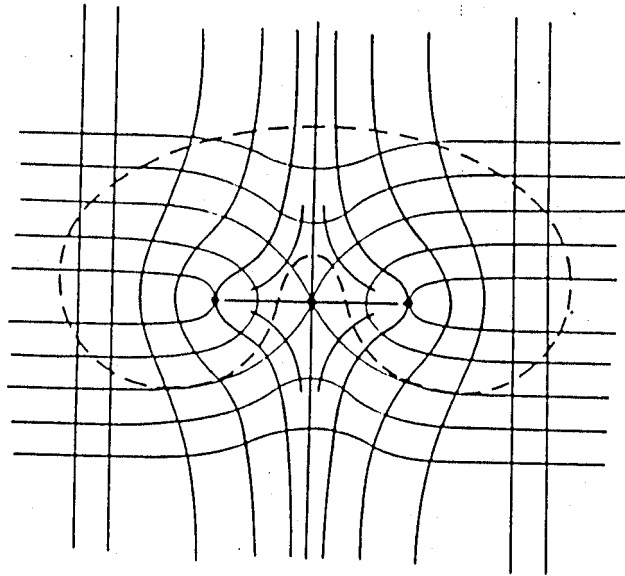


Figure 2.28

A hyperbolic point defect occurring in a smectic A phase being compensated by a singular ring carrying a topologically opposite charge (From Trebin 1982).

angle made by the director with the radius vector.  $\phi$  is the angle made by the director with the x-axis and is equal to  $a - \delta$  in the first and third quadrants, and  $a + \delta$  in the second and fourth quadrants. Let  $\psi$  be the azimuthal angle made by the polariser with the x-axis. The regions of the sample, where  $\phi = \psi$  or  $\phi = \psi + 90^\circ$  are crossed out by the analyser.

Let us consider the following 3 cases:

- 1 When the polariser is parallel (or perpendicular) to the x-axis ( $\psi = 0$ ), regions with the director along the x-axis are crossed out by the analyser, i.e., there is an overall darkening of the sample except within and just outside the  $N_R$  droplets where the director makes an angle with the x-axis in most regions (Fig. 2.29).
- 2 When the polariser makes a small angle (say  $\psi \approx -10^\circ$ ) with the x-axis two brushes are present in the  $N_D$  region outside any  $N_R$  droplet. The exact position of these brushes depends on  $\delta$ . In Fig. 2.30a these brushes can be seen just outside the  $N_R$  droplet. This can be compared with the expected pattern of dark brushes (Fig. 2.30b) obtained from the director configuration shown in Fig. 2.27b for  $\psi = -10^\circ$ .
- 3 When  $\psi \approx -45^\circ$ , four dark brushes (see Fig. 2.31a) are visible outside the  $N_R$  droplets. Two of the four brushes lie very close to the periphery of the  $N_R$  droplet. The expected pattern is shown

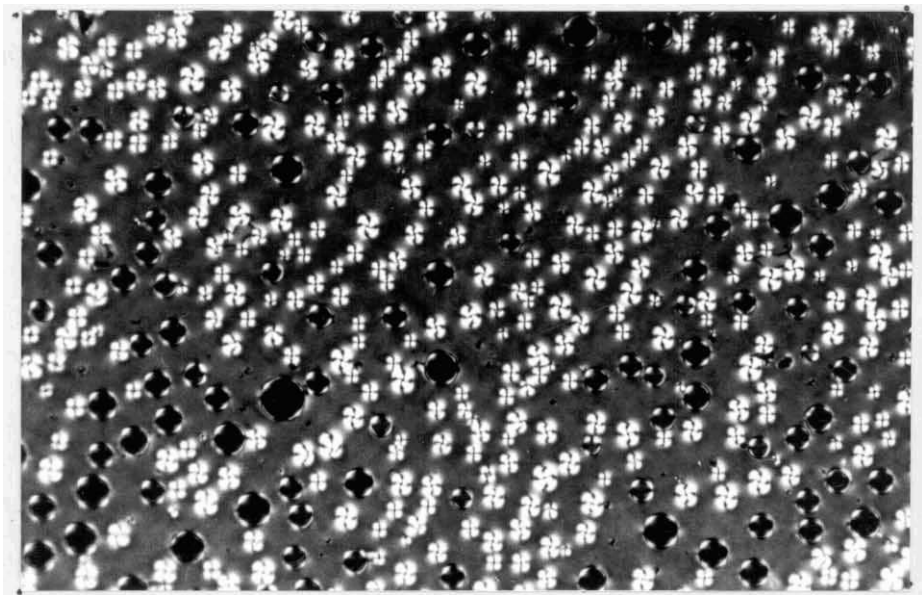


**Figure 2.29.** Coexistence of  $N_R$  and  $N_D$  phases with the  $N_D$  phase aligned along x-axis (lower edge of photograph) in a sample with 30 mol % of  $C_7OHBT$  at  $88^\circ C$ , crossed linear polarizers, and  $\psi = 0^\circ$  ( $\times 450$ ).

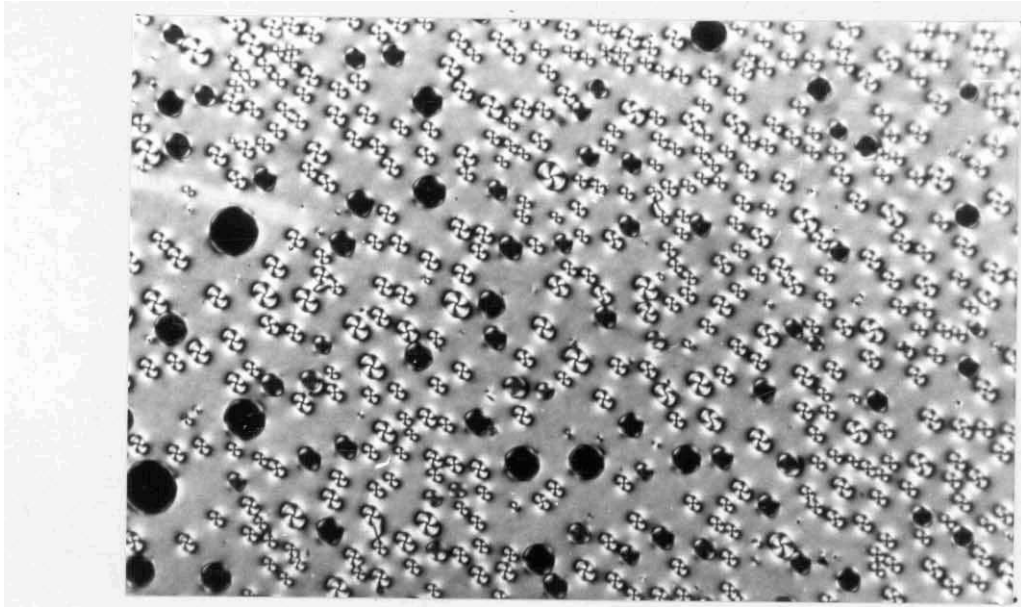


Figure 2.30a. Different area of the same sample as in Fig. 2.29, crossed linear polarisers, with  $\psi \sim -10^\circ$  (x 450)

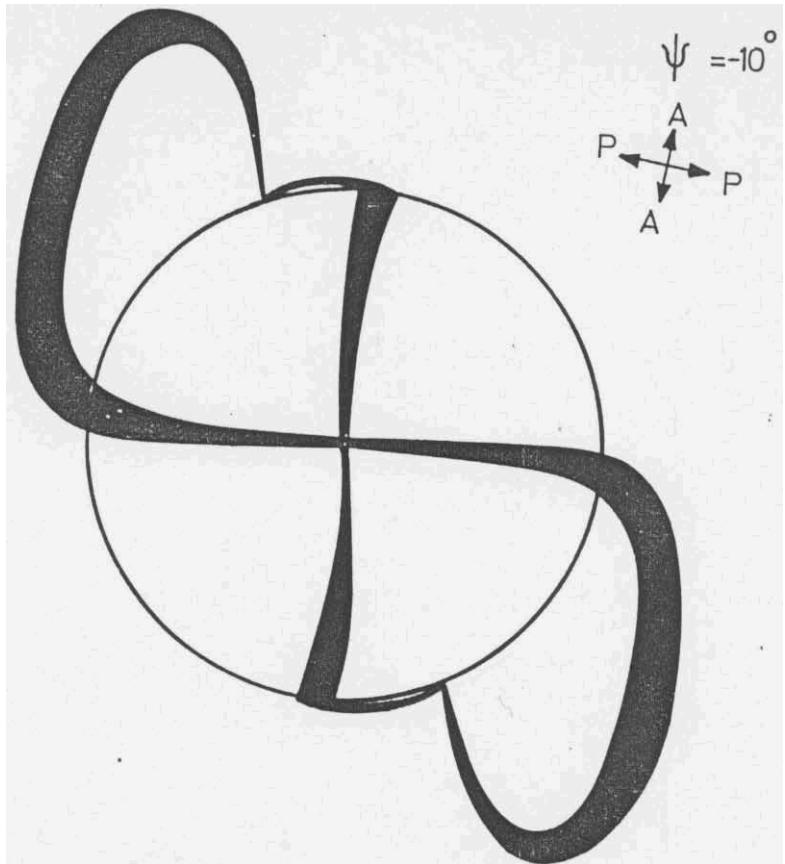


Figure 2.30b

Pattern of dark brushes obtained from Fig. 2.27b for  $\psi = -10^\circ$ .

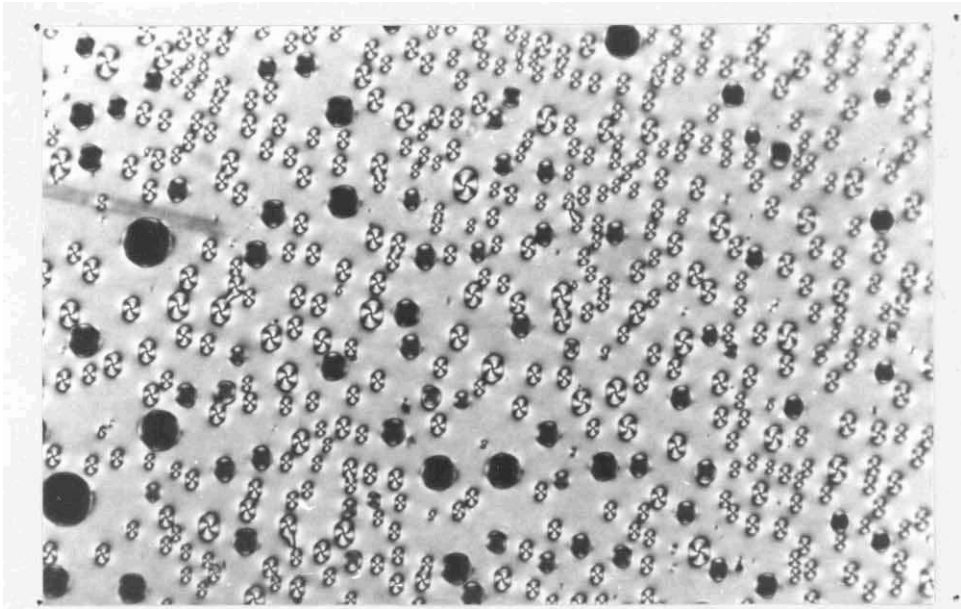
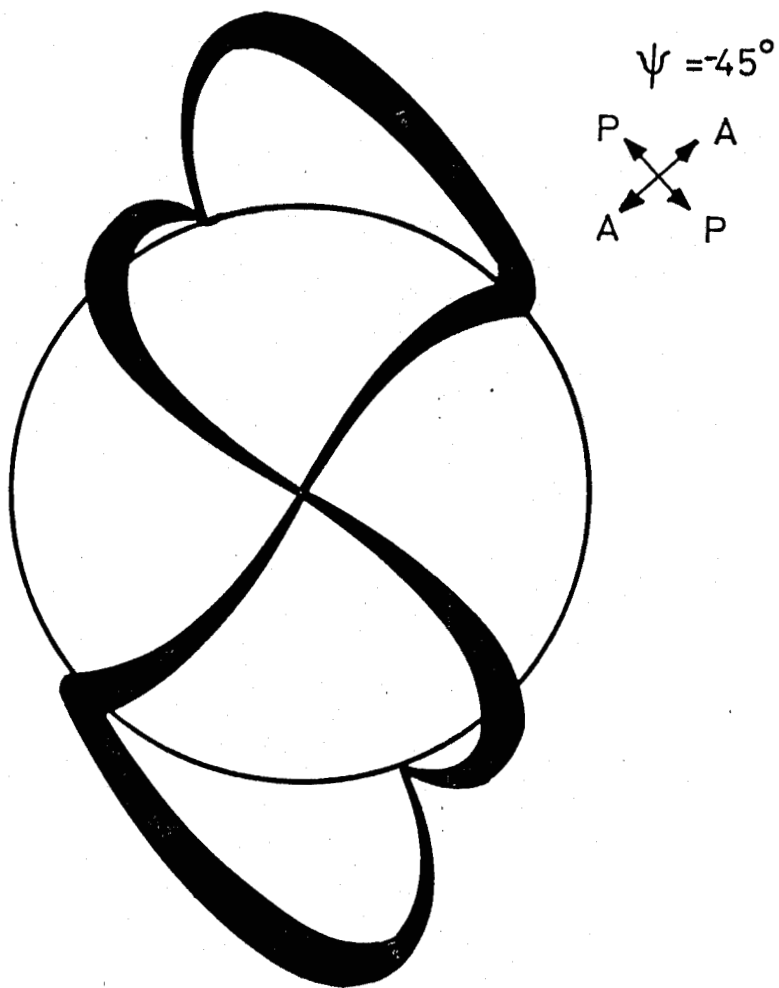


Figure 2.31a. Same sample area as in Fig. 2.30a, crossed linear polarisers,  $\psi \approx -45^\circ$  (x 450).



**Figure 2.31b**

Pattern of dark brushes obtained from Fig. 2.27b for  $\psi = -45^\circ$ .

in Fig. 2.31b obtained from the director configuration given in Fig. 2.27b for  $\psi = -45^\circ$ .

As the sample is cooled the +1 defect is found to move away from the centre of the  $N_R$  droplets. Volovik and Lavrentovich (1983) have found in some systems a variation of the boundary condition of the director from tangential to radial, in nematic droplets suspended in glycerine, as a function of temperature. They find that for an intermediate value of the angle made by the director at the interface the +1 defect can move away from the centre. In the system studied by us, a similar change in the angle made by the director at the interface causes a shift in the position of the +1 defect in the  $N_R$  droplet.

Fig. 2.32a shows a sample which exhibits the coexistence of  $N_R$  and  $N_D$  phases taken between SiO coated plates at  $88^\circ\text{C}$  and viewed between crossed linear polarisers. The +1 defects are seen to be at the centres of the  $N_R$  droplets. Fig. 2.32b shows the same sample area as in Fig. 2.32a when the temperature is lowered to  $80^\circ\text{C}$ . The +1 defects are seen to have moved away from the centres of the  $N_R$  droplets. Fig. 2.33a shows another region with a similar structure. This shift of the +1 defect from the centre can be more clearly seen with circular polarisers. Fig. 2.33b shows the same sample area as shown in Fig. 2.33a viewed between crossed circular polarisers.

## 2.4 CONCLUSION

We have found the coexistence of two nematic phases, one rela-



**Figure 2.32a.** Coexistence of  $N_R$  and  $N_D$  phases in a mixture with 30 mol % of  $C_7OHBT^R$  at  $88^\circ\text{C}$ , sample taken between  $\text{SiO}$  coated plates, crossed linear polarisers (x 450). The point defects are located at the centre of the  $N_R$  drops.



**Figure 2.32b.** Same sample area as in Fig. 2.32a at  $80^\circ\text{C}$ ; the +1 defect in each drop has shifted to one end (x 450).

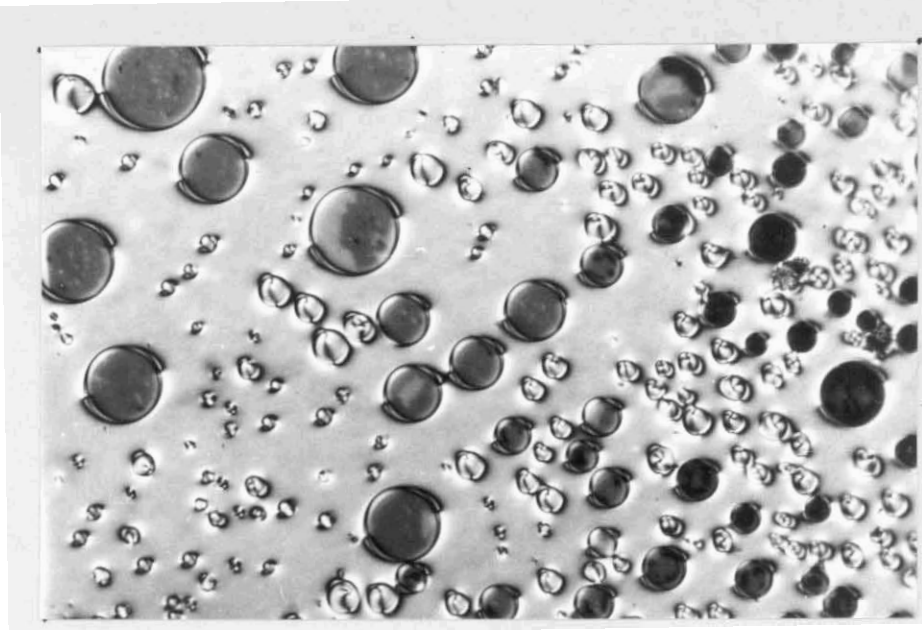


Figure 2.33a. Another region of the same sample as in Fig. 2.32a at  $83.3^{\circ}\text{C}$  with the  $+1$  defect shifted from the centre of  $N_R$  droplets, between crossed linear polarisers (x 450).

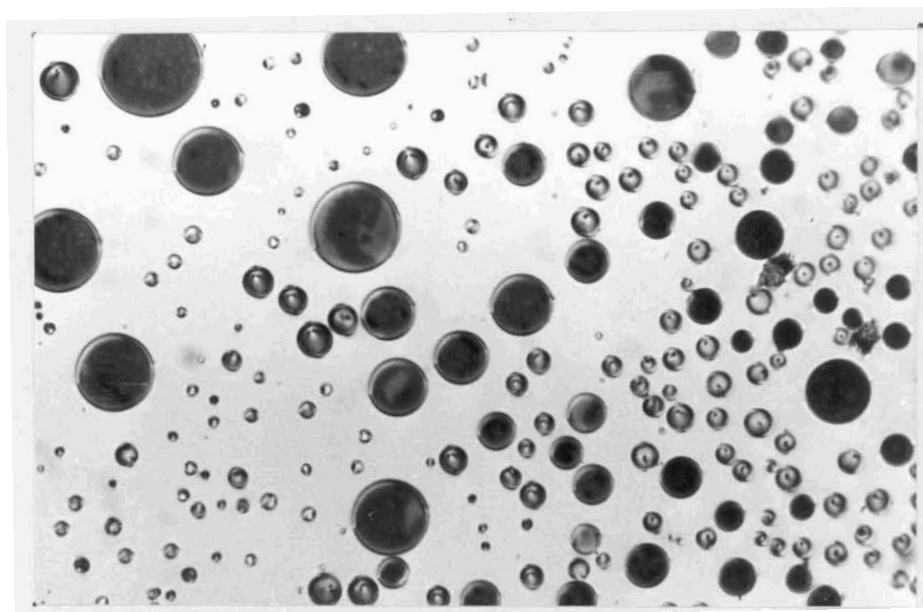


Figure 2.33b. Same area of the sample as in Fig. 2.33a between crossed circular polarisers (x 450).

tively rich in rod-like molecules and the other in disc-like molecules, in mixtures of nematogens with rod-like and disc-like molecules in two systems. When the mixtures that exhibit the coexistence in System I are taken between glass plates coated with SiO the director distortion due to the point defect of strength +1 present at the centres of the  $N_r$  droplets is found to be annulled by a singular ring defect of strength - 1/2 .

## REFERENCES

- Alben, R. 1973 J. Chem. Phys., 59, 4299
- Caflisch, R.G., Chen, Z.Y., Nihat Berker, A. and Deutch, J.M. 1984 Phys. Rev., **A30**, 2562.
- Casagrande, C., Veyssie, M. and Finkelmann, H. 1982 J. de Phys. Lett., 43, L-671
- Chen, Z.Y. and Deutch, J.M. 1984 J. Chem. Phys., 80, 2151.
- Destrade, C., Foucher, P., Malthete, J., Tinh, N.H. 1982 Phys. Letts., **88A**, 187
- Destrade, C., Gasparoux, H., Babeau, A. and Tinh, N.H. 1981 Mol. Cryst. Liq. Cryst., 67, 37
- Dubois-Violette, E. and Parodi, O. 1969 J. Phys., 30, C4-57.
- Hartshorne, N.H. and Stuart, A. 1934 "Crystals and the Polarising Microscope" (Edward Arnold & Co., London)
- Hashim, R., Luckhurst, G.R., Romano, S. 1984 Mol. Phys., **53**, 1535
- Lavrentovich, O.D. and Terentev, E.M. 1986 Sov. Phys. JETP, 64, 1237
- Madhusudana, N.V. and Sumathy, K.R. 1983 Mol. Cryst. Liq. Cryst. Lett., 92, 179
- Mourey, B., Perbet, J.N., Hareng, M. and Le Berre, S. 1982 Mol. Cryst. Liq. Cryst., 84, 193

- Palfy-Muhoray, P., Berlinsky, A.J. and de Bruyn, J.R. 1984 Phys. Lett., **104A**, 159
- Palfy-Muhoray, P., de Bruyn, J.R. and Dunmur, D.A. 1985A J. Chem. Phys., 82, 5294
- Palfy-Muhoray, P., de Bruyn, J.R. and Dunmur, D.A. 1985B Mol. Cryst. Liq. Cryst., 127, 301
- Perez, A., Brunet, M. and Parodi, O. 1978 J. de Phys. Lett., 39, L-353
- Rabin, Y., McMullen, W.E. and Gelbart, W.M. 1982 Mol. Cryst. Liq. Cryst., 89, 67
- Tinh, N.H., Destrade, C. and Gasparoux, H. 1979 Phys. Lett., **72A**, 251
- Tinh, N.H., Gasparoux, H. and Destrade, C. 1981 Mol. Cryst. Liq. Cryst., 68, 101
- Trebin, H.R. 1982 Advances in Physics, 31, 195
- Vauchier, C., Zann, A., Le Barry, P., Dubois, J.C. and Billard, J. 1981 Mol. Cryst. Liq. Cryst., 66, 103
- Volovik, G.E. and Lavrentovich, O.D. 1983 Sov. Phys. JETP, 58, 1159
- Yu, L.J. and Saupe, A. 1980 Phys. Rev. Lett., 45, 1000.